

Fault-zone deformation in welded tuffs at Yucca Mountain, Nevada, U.S.A.

Mary Beth Gray^{a*}, John A. Stamatakos^b, David A. Ferrill^b, Mark A. Evans^c

^a*Department of Geology, Bucknell University, Lewisburg, PA 17837, USA*

^b*Center for Nuclear Waste Regulatory Analyses, Southwest Research Institute, San Antonio, TX 78238, USA*

^c*Department of Physics and Earth Science, Central Connecticut State University, New Britain, CT 06050 USA*

Abstract

Field and microstructural analysis of faults with millimeters to hundreds of meters of displacement within welded tuffs at Yucca Mountain, Nevada, has led us to identify four different fault zone architectures. We designate these fault zones as Classes A, B, C, and D. We conclude that Classes A, C, and D are genetically related and that observed differences in their morphology and deformation mechanisms are related to differences in displacement magnitude and changes in the rheology of faulted rocks. We show that Class A, C, and D fault zones were formed by progressive cataclasis, leading to the development of a foliated gouge core and wide damage zone at the highest displacement magnitudes. By inference, displacement variations across individual high displacement faults are expected to produce significant lateral changes in fault zone architecture. The broad range of fault rock textures and architectures found on the Class A, C, and D continuum may produce important corresponding variability in hydrologic properties in ignimbrites.

By contrast, Class B fault zones have unique mineralogies and microtextures relative to other Yucca Mountain fault zones. Most notable is the occurrence of distinctive jigsaw puzzle texture within fault core breccias, which consists of angular wall rock fragments floating in a coarsely crystalline secondary calcite cement matrix. The calcite cement constitutes more than 65% of the Class B fault zones. Comparisons to other occurrences of secondary minerals within

* Corresponding author. Fax: +1-570-577-3031.

E-mail address: mbgray@bucknell.edu (M.B. Gray).

Phone: 570-577-1146

open lithophysal cavities, which appear to have formed in unsaturated conditions, indicate that the secondary mineralization history at Yucca Mountain was complex and likely polygenetic. The age and origin of the secondary calcite minerals in the Class B fault zones remain undetermined.

1. Introduction

Yucca Mountain, Nevada (Fig. 1a), the potential site for a high-level nuclear waste repository, consists of a ridge of welded and nonwelded pyroclastic flows and air-fall tuffs that erupted from the Southwest Nevada Volcanic Field calderas in the Late Miocene, between approximately 11 and 15 Ma (Sawyer et al., 1994). Tuffs exposed at Yucca Mountain include units of the Crater Flat and Paintbrush Groups as well as the Calico Hills Formation. The repository is currently planned to be housed within moderately to densely welded members of the Topopah Spring Tuff, which is one of the main tuff units of the Paintbrush Group.

Yucca Mountain lies within the southern Great Basin of the central Basin and Range Physiographic Province (Fig. 1b). It is part of the Crater Flat Basin, a half-graben bounded on the west by the east-dipping Bare Mountain fault and on the east by a series of mostly west-dipping faults that are antithetic to the Bare Mountain fault (Fig. 1c). Within this structural framework, Yucca Mountain is a tilted fault block that dips approximately 5-10° to the east (Figs. 2a and 2b). Yucca Mountain is bounded on the west by the Solitario Canyon fault and on the east by the Bow Ridge and Paintbrush Canyon faults (Potter et al., 2004) (Fig. 2b). Most faults within the Yucca Mountain block are steeply dipping normal faults; however, oblique slip, strike-slip, high-angle reverse, and low-angle thrust faults are also present. Growth strata in the Paintbrush Group adjacent to some of the faults indicate faulting initiated before or during tuff deposition (e.g., Day et al., 1998). Faulting activity was most prominent in the Late Miocene between 11 and 12 Ma (Fridrich et al., 1999). Faulting has remained active to the present, as indicated by offset Quaternary deposits across many large faults at Yucca Mountain (e.g., Stepp

* Corresponding author. Fax: +1-570-577-3031.

E-mail address: mbgray@bucknell.edu (M.B. Gray).

Phone: 570-577-1146

et al., 2000) and historic seismicity (e.g., Rogers et al., 1991).

The U. S. Code of Federal Regulations at 10 CFR Part 63 require the potential of Yucca Mountain as a repository to safely contain high-level radioactive waste for 10,000 years. The unprecedented long design life of the facility and the technical challenge of permanently disposing high-level radioactive waste in a geologic repository have prompted the U.S. Department of Energy (DOE) to develop a 10.4-km-long network of tunnels at a maximum depth of 300 m within Yucca Mountain. The Exploratory Studies Facility (ESF) is a 7.6-m diameter, 7.8-km-long tunnel from which the 6.1-m diameter, 2.6-km-long Enhanced Characterization of the Repository Block or Cross Drift tunnel was bored (CRWMS M&O, 1998). Miocene volcanic tuffs of Yucca Mountain are of generally high strength and require minimal structural support, which allow nearly continuous three-dimensional exposures of rock (CRWMS M&O, 1997).

Our analyses of faults and fault zones in the ESF and Cross Drift were initiated in 1998, mainly to refine models of faulting used in the U.S. Nuclear Regulatory Commission (NRC) repository performance assessment codes. Such models are essential to evaluate uncertainties in the performance estimates from potential direct disruption of the emplaced waste by fault movements. Accurate models of faulting require a detailed description and understanding of faults at the repository host-horizon level (Gray et al., 1998; 1999). Results of our fault studies from the ESF and Cross Drift also bear on other components potentially affecting repository performance. In particular, our study provides important constraints for hydrologic models and interpretations of groundwater thermochronology at Yucca Mountain (Gray et al, 2000).

The ages, origins, and significance of secondary mineralization at Yucca Mountain have been the subject of debate for more than a decade. Much of the most recent research has centered on the textures, isotope geochemistry and fluid inclusion microthermometry in mineral occurrences within lithophysae and fractures (e.g., Paces et al., 2001; Whelan et al., 2002; Wilson et al., 2003). Based on these occurrences, Paces et al. (2001) concludes that the repository horizon has been within the vadose zone since deposition of the tuffs. They point out that most lithophysal cavities are unfilled or only partially filled with secondary minerals and

that mineralization is generally restricted to the floors of the cavities. Strontium, oxygen, and carbon isotopic signatures have been interpreted by these researchers to indicate the source of calcium carbonate was meteoric water from above throughout the postdepositional history of the tuffs (Whelan and Moscati, 1998; Paces et al., 2001; Whelan et al., 2002; Wilson et al., 2003). A comprehensive fluid inclusion microthermometry study on samples collected in the ESF and Cross Drift yielded homogenization temperatures (equivalent to tapping temperatures in this case) for two-phase primary fluid inclusion assemblages within calcite averaging between 45 and 60°C and reaching a maximum of 83°C. In contrast, Dublyansky et al. (2001) conclude that at least some of the secondary minerals found in lithophysal cavities were precipitated from water with elevated temperature derived from below Yucca Mountain. They suggest that warm water invaded the repository horizon several times in the past and potentially in the recent past. Dublyansky et al. (2001) pointed out that two-phase fluid inclusion assemblages, some containing evidence of hydrocarbons, are present in calcite. Our observations of fault-related mineralization must be examined in light of existing conflicting interpretations of the history and significance of secondary mineralization at Yucca Mountain. Although our results do not resolve the ongoing debate, they provide additional information that should be addressed and incorporated in models of secondary mineralization at Yucca Mountain.

Our approach for gaining a better understanding of faulting was to examine, in detail, the fault rocks that comprise the fault zones. Fault-zone deformation in the upper crust produces a wide variety of morphologies indicative of the conditions and history of faulting. Idealized faults consist of two textural zones, a fault core and a damage zone (Caine et al., 1996; Seront et al., 1998). The fault core is a zone of relatively high strain that typically accommodates most of the fault displacement by shear in gouge, cataclasite, breccia, or mylonite. The surrounding damage zone is less deformed, accommodates less displacement, and contains subsidiary structures such as joints, veins, and minor faults. The dimensions of a fault zone are typically expressed in terms of thickness (measured normal to the fault zone boundaries) or width (measured horizontally between fault zone boundaries).

Deformation mechanisms govern the behavior, textural morphology, and ultimately, the

gross architecture of fault zones. At Yucca Mountain, the protolith (welded volcanic tuff) has undergone brittle deformation dominated by cataclasis at shallow levels in the upper crust. Changes in deformation mechanisms with time and increased fault displacement, the presence or absence of fluids in the fault zone, mineral transformations, and syndeformational mineralization affect the rheology of the fault zone, causing the active parts of the faults to widen or narrow with increasing displacement. Two-end member possibilities exist (Wojtal and Mitra, 1986), (1) deformation produces fault rocks that inhibit further slip in the fault core (i.e., strain hardening) so additional fault displacement causes the protolith to fracture and the fault zone to widen with time, and (2) the fault rocks become progressively easier to deform (i.e., strain localization or strain softening) so deformation is localized to a progressively narrower portion of the fault zone. In strain softening, the intensely deformed fault core incrementally accommodates more of the deformation, and there is no further increase in fault-zone width. Investigations of faulting at Yucca Mountain, especially studies of fault zones exposed in the ESF, reveal that all of these deformation processes and related features are present, and subsets of fault zones with common architecture may be defined on the basis of this approach.

In this paper, we present results from detailed observations of fault zones exposed within Yucca Mountain. In particular, we present our findings of four different fault zone architectures, which we denote as Classes A, B, C, and D. Based on those observations, we interpret the genetic relationships between different fault zone types. The ramifications of these findings are then discussed in light of ongoing studies of secondary mineralization, paleohydrology, and groundwater thermochronology at Yucca Mountain.

2. Fault zones exposed in the underground excavations

Our study examined faults on the ground surface, in trenches, in cores (VH2, USW-G1, and USW-G2), and in the ESF and Cross Drift. Our sampling strategy sought to document the variability of fault zone architecture. As a result, the proportions of different fault zone classes in our sample collections are not representative of the relative abundances of these fault zone

classes within Yucca Mountain. Most fault rock samples were vacuum impregnated with epoxy prior to thin-section preparation. Samples were precisely oriented and cut along two mutually perpendicular directions. Transverse thin sections were cut normal to the fault plane and parallel to the dip direction of the fault. Longitudinal thin sections were cut parallel to the strike of the fault and normal to the fault plane.

We prepared and examined 32 core, 32 surface and trench, and 117 ESF and Cross Drift thin sections. Thin sections from core samples provided useful ancillary information but because of their small size and limited orientation information, the larger scale fault architecture could not be deciphered from the cores alone. Samples from the surface and trench exposures are typically indurated with caliche, opal, and sepiolite (Hill et al., 1995; Dublyansky et al., 1998; Stuckless et al., 1992). Mineralization dominates the fault rocks, making it difficult to determine the original fault rock fabrics or distinguish cemented surficial deposits from fault rock breccias. Some mineralization is clearly caused by pedogenic surficial processes (e.g., root traces are present in some samples) although the total extent of pedogenic overprint is unclear and disputed (e.g., Hill et al., 1995; Stuckless et al., 1998). ESF and Cross Drift fault samples are further from the surface and less likely to contain a pedogenic overprint. For all of the reasons outlined above, this paper principally relies on the ESF and Cross Drift thin-section analyses and field observations.

We recognize four broadly defined classes of fault zone architecture (Fig. 3). For ease of discussion, we refer to these as Class A, B, C, and D fault zones, in order of generally increasing displacement. We recognize that displacement can vary with position along a single fault and that it is possible that fault zone architecture within a given fault zone may be different if observed at the surface or in cores from deeper in Yucca Mountain. In general, fault zone thickness increases as faults approach the ground surface at Yucca Mountain. For example, the Ghost Dance fault core is 1 m wide in the ESF and >10 m wide (measured along a horizontal transect) 300 m above at the surface. Displacement changes dramatically (1 to 30 m) along strike (Mongano et al., 1999). Narrow fault zones (<1 m wide) and faults with displacements of <3 m constitute the majority of the faults in the Yucca Mountain ESF (CRWMS M&O, 1998;

Fig. 4).

2.1. Class A

Class A fault zones are discrete slickensided fractures with minor displacements and little or no damage zone. Class A fault zones have displacements of millimeters to a few centimeters. Slickenlines and slickensides (Fleuty and Weaver, 1975) are common. Damage zones are <2 cm wide, and if present, fault cores do not exceed 1 cm in width (Figs. 3a and 5a). Secondary minerals, such as chalcedony, are present in thin films in the fault cores of some Class A fault zones. Microscopic examination of Class A damage zones confirm that the damage zone is composed of subsidiary, discontinuous microfractures and microfaults with submillimeter scale offsets. In those Class A fault zones that contain secondary minerals, the minerals do not appear to be offset by displacements of the core/damage zone boundary. The crystals show no evidence of deformation, and the deposits simply fill in the relief formed by submillimeter scale subsidiary fault offsets. Class A fault zones appear to have been formed by brittle fracture of the protolith, frictional sliding, and propagation of subsidiary fractures and faults. Some Class A fault cores are partially to completely mineralized while other Class A fault cores remain unmineralized. Where secondary minerals are present, there is no indication of brittle fracturing, crystal plastic deformation, or pressure solution of the secondary minerals that would indicate fault slip after mineralization. We therefore interpret the secondary minerals in Class A fault zones to be post-kinematic.

2.2. Class B

2.2.1 Description

Class B fault zones are characterized by thin, mineralized, brecciated cores and poorly developed damage zones. The boundaries between Class B cores and damage zones are

slickensided. Class B fault zones (Fig. 3b) have displacements of <1 m with the notable exception of one of the two main splays of the Drill Hole Wash fault (Appendix A). Based on extrapolation from slickenline orientations and fault dip separation, the Drill Hole Wash fault splay may have 14 m oblique net slip in the ESF North Ramp. Faults containing Class B fault zone architecture generally strike NW-SE. Class B fault zones are similar to Class A fault zones in that they have either poorly developed damage zones, limited to a few centimeters wide, or in some cases, have no damage zone at all. Class B fault zones contain a well-developed fault core between 2 and 30 cm thick, averaging 7 cm in thickness (Fig. 5b). Core thickness varies laterally and vertically both up and down dip. Thickness variations are most commonly associated with dilational jogs.

The fault core boundaries are typically discrete, slickensided, and can contain multiple slickenline orientations, among which low- and high-rake slickenlines are most common. One fault core sample from ESF Station 43+39 contains two slickenline orientations on the core-damage zone boundary, one oblique and one horizontal. The oblique slickenlines emanate from and are localized by ridges formed by the strike-parallel set, indicating that the strike-parallel set predates and localized the formation of the younger, oblique set. Calcite strain gauge analysis (Groshong 1972, 1974; Evans and Groshong, 1994) of this core sample indicates a right-lateral strike-slip history for the Class B fault at ESF Station 43+39 (Fig. 6a), consistent with the observed strike-slip slickenlines. Apparently, the younger, oblique-slip event was localized along the core damage zone boundary and did not involve crystal plastic deformation of calcite in the fault core. The nearly vertical intermediate principal extension and nearly horizontal maximum and minimum principal extensions in the fault sample from drill core samples 02016200 (Fig. 6b) are consistent with deformation in a strike-slip strain field. The nearly horizontal maximum principal extension and oblique maximum and intermediate principal extensions in the fault from drill core sample 02016201 (Fig. 6c) imply a transitional strain field between extensional and strike slip.

Class B fault cores consist of angular rock fragments and as much as 65% or more calcite matrix (Fig. 7a). The clasts are relatively intact and show little evidence of comminution. Most

wall rock tuff fragments contain undisturbed eutaxitic foliation, indicating that little progressive cataclasis occurred after initial brecciation of the tuff fragments and entrainment in calcite. Tuff fragments are commonly angular and elongate, creating tabular- or rectangular-shaped clasts (Fig. 7a). Despite the strong mechanical anisotropy created by the eutaxitic foliation (CRWMS M&O, 1997), the flat planar boundaries of the clasts are commonly at high angles to the eutaxitic foliation within the clasts (Figs. 8a and 8b). This angular relationship suggests faulting initiated by closely spaced brittle fracturing subparallel to the fault zone boundaries. The dispersion of rock fragments is perhaps best described as an exploded jigsaw puzzle breccia (Sibson, 1986) or jigsaw breccia (Seront et al., 1998). Some clasts can be graphically restored to fit into one another by simple rigid body translation and/or rotation. This fault rock texture requires significant dilation across the fault zones (beyond that needed during initial fault brecciation) but is not restricted to the dilational jogs within exposed Class B fault zones.

Tuffaceous wall rock clasts are supported by calcite matrix with crystals ranging from coarse (e.g., 0.5-cm diameter) to microcrystalline. The large patches of crystallographically continuous calcite are similar to poikilotopic cements observed elsewhere in carbonate rocks (e.g., Folk, 1974; Scholle and Ulmer-Scholle, 2003). Low-temperature crystal-plastic deformation of calcite caused development of abundant mechanical twins and intragranular fractures that offset twins and grain boundaries (Figs. 7a, 7b, and 7c). A calcite strain gauge analysis of one Class B fault core indicates deformation by mechanical twinning accommodated a 2.24% extension (Appendix A). Calcite crystals are offset by less common transcrystalline fractures. Transcrystalline shear fractures are confined to the crystalline matrix and do not crosscut wall rock clasts. Although intercrystalline shear fractures and crystal plastic deformation is evident within fault cores, much of the deformation appears to have been localized by frictional slip at the fault core boundaries. Initiation and development of the calcite matrix textures in Class B fault cores are problematic. Wall rock inclusion trails, abundant transcrystalline shears, and closely spaced planes of secondary fluid inclusions indicative of a crack-seal mechanism of fracture dilation were not observed. The calcite is not cathodoluminescent and does not appear to be growth zoned. Class B fault zone textures have

textural features that are characteristics of implosion breccias described elsewhere (Sibson, 1986, 1994; Muechez and Sintubin, 1998; Seront et al., 1998). Implosion breccias form during faulting by rapid decrease in pore fluid pressure at dilational jogs with a resulting fluid pressure differential that exceeds the tensile strength of the rock (Sibson, 1986, fig. 2c). Implosion breccias are known to have exploded jigsaw puzzle breccia textures; wall rock clasts have little internal deformation and are commonly matrix supported (Sibson, 1986, 1994; Seront et al., 1998). Implosion breccias may form in a variety of structural settings (e.g., Zhang and Sanderson, 1996; Muechez and Sintubin, 1998; Seront et al., 1998) but are not expected to form at depths less than approximately 500 m (Sibson, 1986). The matrix-supported crystalline breccia texture and dearth of crack seal textures suggest that initial crystallization of the calcite matrix in Class B fault cores accompanied fault rupture and may have occurred rapidly. In this interpretation, the CaCO₃-saturated fluid would be integral to the faulting process, and mineralization of the crystalline matrix would be synkinematic.

Poikilotopic cements in sedimentary rocks are attributed to slow nucleation and growth rates (Folk, 1974; Tucker and Wright, 1990) and/or cement recrystallization (Friedman, 1965; Chafetz et al., 1985). Because the textural evidence supports rapid crystallization of a synkinematic calcite matrix, we interpret the poikilotopic texture we observe in some Class B faults to indicate recrystallization of the matrix. Because the poikilotopic calcite contains abundant deformation twins, the recrystallization was probably synkinematic as well. Class B fault cores also contain rare (< 5 mm thick) veins, partially or entirely filled with relatively strain-free and inclusion-free calcite (Fig. 7d). These veins cut across the recrystallized, deformed core matrix and are, therefore, interpreted to be postkinematic. Veins are subparallel to the fault zone boundaries, indicating late-stage dilation at a high angle to the fault zone boundaries.

2.2.2 Mechanical twinning of calcite matrix and temperatures of deformation

Experimental and field-based studies demonstrate that the thickness of mechanical twins

(sometimes referred to as “deformation twins”) on the *e* plane in calcite correlates with the temperature at which calcite deformed (Ferrill, 1991, 1998; Burkhard, 1993). Mechanical e-twinning of calcite is the dominant crystal-plastic deformation mechanism in coarse-grained limestone and marble deformed at temperatures below approximately 400 °C (Turner, 1953; Carter and Raleigh, 1969; Groshong, 1988). Definitions of thin-versus-thick calcite twins are given by Groshong (1974). Thin twins appear in thin sections as black lines when observed using a universal stage at 200 to 400× magnification. The black line that constitutes a thin twin in an optical microscope includes a combination of twinned material and the optical effect of the twin boundaries (see Appendix A for further discussion). Thick calcite twins can be resolved optically from the untwinned host. Under cross-polarized light, the calcite within a thick twin can be seen to go to extinction in a different position from that in the untwinned host calcite. Widths of thick twins are measured as the distance between the inner edges of the visible twin boundaries.

As described by Ferrill (1991) and Ferrill et al. (2004), deformation microstructures in calcite are dominated by thin twins <170°C and thick twins >200°C. Calcite deformed at temperatures <170°C accumulates strain by the formation of new thin twins rather than by twin enlargement or the formation of thick twins. At higher temperatures, a larger proportion of thick twins forms to accommodate increased strain, and thermally activated twin boundary migration further increases the mean observed twin width. At >200°C, most twins are large enough to be classified as thick twins (Burkhard, 1993), and mean twin widths are commensurately larger. Strain accumulation at temperatures >200°C is accomplished by the formation of thick twins and the enlargement of existing twins rather than by thin twin formation. Twin intensities in rocks deformed above 200°C rarely exceed 40 per millimeter (Fig. 9).

Calcite twin analysis was performed on three samples of Class B fault rock containing coarsely crystalline calcite from Yucca Mountain. This analysis was performed following methodologies outlined in Ferrill (1991) and Ferrill et al. (2004) (Appendix A). Comparing twin strain determined from the calcite strain gage technique, mean twin widths, and mean twin intensities from the three calcite twin samples from Yucca Mountain fault rocks with data from

the Alps and Appalachians (described by Ferrill et al., 2004) shows that the Yucca Mountain samples plot in the general field with rocks deformed at temperatures of 170–200°C, or >200°C (Fig. 9). The pattern of Yucca Mountain data clearly does not plot in the graphical region occupied by samples deformed at <170°C. Individual twins in the Yucca Mountain samples are in many cases quite thick (as much as 12 microns), and 83% of the measured twins from the three Yucca Mountain samples are classified as thick twins, having measurable widths of twinned material at 400× magnification using an optical microscope. Together these data support the conclusion that twinning occurred at relatively elevated temperatures of >170°C.

We have identified two-phase fluid inclusions in the sparry calcite from Class B fault core matrix, which may be eligible for collecting fluid inclusion microthermometry data. Calcite fluid inclusion microthermometry in fault rocks must be used with caution because of the potential for post-entrapment modifications of inclusions which could influence microthermometry results. We plan to explore further the potential for application of fluid inclusion microthermometry to calcite in Class B fault rocks.

2.3. *Class C*

Class C fault zones are found in faults with a wide range of displacements (spanning four orders of magnitude) and comprise correspondingly variably thick, well developed brecciated cores and intensely fractured damage zones. Class C fault zones (Fig. 3c) have displacements of a few centimeters to tens of meters and have correspondingly well-developed fault cores ranging from tens of centimeters to 1 meter thick. These fault zones are from all slip classifications (normal, strike slip, and reverse). The Ghost Dance fault exhibits Class C fault zone characteristics, as do thrust faults found within the ESF (Fig. 5c). Minor slickensided fractures typically bound Class C fault zone cores. Damage zones range from 1 to 10 m thick. Fault cores consist of noncohesive to poorly cohesive, unfoliated cataclasite and breccia (Fig. 7e and 7f). Fault cores contain antithetic and synthetic faults that connect floor to roof of the cores or tie into other minor faults, giving a macroscopic appearance of slickensided blocks of cataclasite/breccia

within the fault core. In thin section, fault cores are composed of unfoliated cataclasite bounded by discrete intergranular sliding surfaces. The cataclasite is composed of tuffaceous wall rock fragments and clasts of cataclasite ranging from submicroscopic to several centimeter in diameter. Tuff fragments are angular to subrounded and slightly elongate to equant. In contrast to Class B faults (Fig 8a), the modal orientation of the long dimension of the clasts in Class C faults is subparallel to the eutaxitic foliation (Fig. 8c). Fractures that bound clasts exhibit a wide variety of orientations relative to the primary foliation in the clasts (Fig. 8d). When compared to the Class B fault zone clasts, Class C fault zone clasts appear to have a higher proportion of clast-bounding fractures subparallel to the primary foliation (Fig. 8b and 8d). Secondary mineralization in Class C faults is volumetrically minor. In contrast to the postkinematic mineralization in Class A faults, small chalcedony veins within Class C fault zones are offset by transgranular shears (Fig.7g).

Class C fault zones appear to have formed by cataclasis and frictional sliding between clasts in the fault core. Progressive clast size reduction occurred by frictional wear, brittle fracturing of clasts, preferentially subparallel to the eutaxitic foliation, and by transgranular sliding between irregular packets of cataclasite.

2.4. Class D

Class D fault zones are found in high displacement fault zones and comprise a composite core of foliated gouge and breccias surrounded by a wide, well-developed damage zone. Class D fault zones (Fig. 3d) have 10 m to hundreds of meters in displacements. These fault zones have wide fault cores and damage zones up to tens of meters in width. Examples of Class D fault zones are the Solitario Canyon fault zone in the cross drift (~300-m dip separation, Mongano et al., 1999) and the Dune Wash fault zone in the South Ramp of the ESF (52-m dip separation, Eatman et al., 1997). Fault cores are composed primarily of poorly cohesive breccia with a cohesive, foliated gouge at or near the center of the core (Fig.5d). The breccia surrounding the gouge varies from being partially mineralized with silica phases and calcite to being

unmineralized. The breccia clasts are composed of comminuted fault rock and may be enveloped by slickensided surfaces. X-ray diffraction analyses confirm the Solitario Canyon fault gouge contains smectite, possibly the product of translocated, altered tuffs (Levy et al., 1999). This gouge is 2 to >8 cm thick and contains a composite foliation (Fig. 7g). One foliation lies parallel to the gouge boundary and one lies at 40° and is synthetic to the main shear direction. Gouge in the Dune Wash fault zone has three foliations: one fault-parallel set of shears, one very prominent phyllosilicate-preferred orientation foliation at 30° to the fault [dihedral angle opens in the direction of shear; “P-foliation,” (Rutter et al., 1986)], and a more widely spaced, well-developed synthetic foliation at 20° to the fault [Riedel shear or R-foliation (Rutter et al., 1986)]. The P-foliation is asymptotic into the Riedel shears and fault-parallel shears. The foliations wrap around survivor grains and exhibit both σ - and δ -type tails (Passchier and Simpson, 1986), indicating clasts underwent rotations during shear of the gouge. Field and microstructural relationships suggest Class D fault zones underwent cataclastic flow in the fault core and brittle fracture accompanied by some polymineralic secondary mineralization in the damage zone.

Some cooling joints elsewhere in the ESF and Cross Drift have 2–4-cm-thick fillings of translocated swelling clays. These cooling joints have been reactivated and have undergone minor amounts of displacement (Sweetkind and Williams-Stroud, 1996). The clays are organized in a similar fashion to Class D gouge containing a well-developed P-foliation, suggesting that large displacements are not required to develop a P-foliation in the clay-rich fracture fill.

3. Origin and significance of fault zone classes

3.1 Class A, C and D fault zones

We interpret that Class A, C, and D fault zones are genetically linked and represent progressive stages of fault zone development (Fig. 10a and b). This progression includes

progressive grain size reduction and clay development associated with increased fault displacement.

Class A fault zones accommodated deformation by brittle fracturing and cataclastic flow within their narrow cores. We interpret that, with increased displacement in a Class A fault zone, clast size was reduced. The fault core underwent strain hardening, and the Class A fault zone widened to form a Class C fault zone (Fig. 10a and 10b). Further displacement then promoted alteration of volcanic rocks to smectite and translocation and recrystallization of clays in part of the fault core, as observed in the Class D fault zones. The smectite weakened the fault core, localizing most of the subsequent displacement to a narrow zone of foliated gouge. Although cataclastic flow in Class A, C, and D fault zones may intrinsically require a small component of fault zone dilation because of rigid body rotation of tuff fragments in the fault core and disorganization of the rock because of cataclasis, we do not consider these fault zones to be significantly dilational.

A positive correlation between fault displacement and fault zone thickness is observed in the ESF and Cross Drift at Yucca Mountain. This general relationship conforms with compilations of field data from other localities (e.g., Hull, 1988; Evans, 1990; Knott, 1994). Because individual faults at Yucca Mountain have variable displacements both with depth and along strike (CRWMS M&O, 1998), it is reasonable to assume that faults with large maximum displacements would exhibit a range of fault zone architectures that correspond with lateral variations in displacement (Fig. 10a and 10b). Within one such large fault, we envision the fault zone might have Class D characteristics in the area of greatest displacement and laterally or vertically transition to Class C and Class A architectures with decreasing displacement toward the fault tip line. Examples of lateral variations in fault zone architecture along individual faults are well documented in the literature (e.g., Sibson, 1986; Kim et al., 2003). Lateral variations in fault zone architecture in ignimbrites may also be produced by spatial heterogeneities in the degree of welding (Wilson et al., 2003).

3.2 Class B fault zones

Because the characteristics of Class B fault zones are sufficiently different from all other classes, it is difficult to conceptualize their having formed within the same evolutionary sequence as Class A, C, and D fault zones. Class B fault zones are significantly dilational and highly mineralized. Fault zone textures and architecture do not support evolution of Class B fault zones from Class A fault zones with increased displacement. Class C and D fault cores do not contain any recognizable characteristic elements of Class B fault cores and, therefore, do not appear to be part of the same genetic continuum as Class B fault zones. There is a possibility or even likelihood, that the steep fault dips (70–90°) and degree of dilational slip observed in the Class B fault zones resulted from hybrid failure (Ferrill and Morris, 2003) [e.g., failure that is transitional between tensile and shear failure (Ramsey and Chester, 2004)]. Typical hybrid failure is observed at shallow depths with relatively low differential stress consistent with the shallow depths where Class B fault zones have been found at Yucca Mountain.

The mineralization in Class B fault zones is distinctive when compared to other occurrences in Yucca Mountain. Lithophysal cavities contain diverse crystal forms of calcite and other minerals interpreted to record a protracted history of characteristically polymineralic secondary mineralization (e.g., Neymark and Paces, 2000; Paces et al., 2001; Neymark et al., 2002). Initial calcite growth occurred at elevated temperatures ($\leq 83^{\circ}\text{C}$) and was followed by growth of minerals that reflect gradual cooling (Wilson et al., 2003). Many of these workers interpreted the lithophysal cavities to record vadose conditions (Cline and Wilson, 2001; Paces et al., 2001; Whelan et al., 2002; Wilson et al., 2003). In contrast, secondary minerals in Class B fault zones have coarse sparry or mosaic calcite matrix textures more indicative of phreatic conditions (Land, 1970; Flugel, 1982; Beach, 1995). Poikilotopic textures exhibited in Class B fault rocks are not known to develop within the vadose zone (Chafetz et al., 1985). Partially filled, postkinematic calcite veins that transect fault cores exhibit void-filling, drusy textures, also indicative of saturated conditions (e.g., Flugel, 1982). Further, the coarse sparry, unzoned, nonluminescing calcite textures in Class B fault rocks do not easily match descriptions given for any of the stages of mineralization previously recognized at Yucca Mountain.

Class B fault cores have sparry calcite with poikilotopic texture suggestive of recrystallization. The sparry calcite contains mechanical twins indicative of deformation at temperatures $>170^{\circ}\text{C}$. As described in the preceding sections, the sharp difference between calcite mineralization in Class B fault zones compared to the mineralization in lithophysal cavities leads us to conclude the thermal and hydrologic history of Yucca Mountain was complex (involving saturated conditions and elevated deformation temporal in some faults) and the origin of the secondary calcite was polygenetic. Either Class B fault zones once served as fluid-saturated conduits while the surrounding rocks remained unsaturated or the faults and surrounding rocks were once saturated at some point in their history and were subsequently deformed at temperatures in excess of 170°C .

Thermal-hydrologic-mechanical processes that can explain this complex and polygenetic mineral history remain elusive. If we assume that faults with the Class B fault zones formed shortly after caldera eruptions and deposition of the tuffs (11–15 Ma), then fault-related mineralization observed in Class B fault cores could be explained by circulating hot fluids related to contemporaneous volcanic-geothermal activity. Alternatively seismically activated episodes have been proposed to explain secondary mineralization and fluid inclusion temperatures as high as 85°C (e.g., Hill et al., 1995; Dublyansky et al., 2001), but their occurrences are highly controversial (c.f., Dublyansky et al., 2001, with Paces et al., 2001). Geologic evidence of hydrothermal activity at Yucca Mountain within the past 10 Ma sufficient to develop the Class B fault zones with calcite-twin deformation temperatures above 170°C is, at best, equivocal (cf. Dublyansky et al., 2001, with Wilson et al., 2003).

Unfortunately, the absolute age of faults containing Class B fault zones, or their age relative to other faults or secondary minerals in lithophysal cavities, is unknown. We observed a very limited set of cross-cutting relationships in the ESF and Cross Drift. Of the five cross-cutting relationships noted, only three suggest that NW-trending faults (such as the majority of faults with Class B fault zones) predate N-S or NE trending faults. This lack of relative or absolute age control on Class B fault zones limits our ability to interpret their origin within existing thermal-hydrology models of Yucca Mountain.

4.0 Hydrologic considerations

A primary control on the permeability structure of stratified rocks is the difference in permeability of sequential rock layers. If the stratigraphic sequence is undeformed, the vertical heterogeneity and anisotropy will dominate the permeability structure. However, groundwater temperature variations (Brikowski, 1997) and hydraulic head differences in the deep aquifer beneath Yucca Mountain (Bredehoeft, 1997) indicate that faults significantly affect the present-day hydrology of Yucca Mountain (Painter and Winterle, 2003). Faulted aquifers, such as those at Yucca Mountain, are influenced by; (i) aquifer communication between fault blocks (Allan, 1989), (ii) fault rock fluid barriers and pathways (Caine et al., 1996; Bredehoeft, 1997; Seront et al., 1998; Caine and Forster, 1999; Ferrill et al., 2000; Ferrill and Morris, 2003), (iii) permeability anisotropy caused by minor fault arrays (Eichhubl and Boles, 2000; Ferrill et al., 2000), and (iv) enhanced permeability caused by dilation of faults responding to contemporary stress (Finkbeiner et al., 1997; Ferrill et al., 1999; Ofoegbu et al., 2001).

The precise architecture of a fault zone may have a significant impact on permeability (Evans et al., 1997). Fault cores may have lower permeability than the protolith because they can form by grain-size reduction, primary porosity reduction, mineral transformations, and secondary mineralization. At shallow levels of the crust, the gouge or cataclasite, therefore, is expected to have relatively low permeability and may effectively form a barrier to fluid flow (Goddard and Evans, 1995; Caine et al., 1996). In contrast, damage zones may have enhanced permeability caused by fracturing and subsidiary faulting (Evans et al., 1997). Coarse-grained, unmineralized fault cores and/or damage zones consisting of open fractures may have greater permeability than the protolith and behave as fluid conduits (Chester and Logan, 1987).

Our four classes of fault zone architecture can be placed within a hydrologic classification scheme devised by Caine et al. (1996). Class A fault zones, with their discrete sliding surfaces and narrow damage zones may be localized conduits. Class C faults zones have intensely fractured damage zones, and cores consisting of unfoliated cataclasite and gouge. These

characteristics may constitute a distributed conduit for fluid flow both across and along the faults. Class D fault zones are the most complex. Their well-developed damage zone is likely to have enhanced permeability relative to the intact host rock while the foliated smectitic gouge is likely to have significantly reduced permeability (Rowling et al, 2001). The net effect is a combined conduit-barrier system (Caine et al, 1996). Bulk anisotropy in fault zone permeability arises as fault-parallel flow is focused in the damage zone between the clay-rich core and relatively intact welded tuff protolith (Evans et al., 1997). Class B fault zones have well-developed mineralized cores and poorly-developed damage zones. The volume of calcite matrix in Class B fault breccias and later stage, low-strain calcite-filled veins subparallel to the fault zone boundaries indicate that these narrow fault zones underwent significant dilation during faulting. Textures suggestive of saturated conditions within the fault core indicate Class B fault zones were fluid conduits when they formed. Fluids may have assisted the faulting process by initiating fault rupture and subsidiary fracture propagation by hydraulic means. Once crystallized, the calcite served to weaken the fault rock as the calcite underwent mechanical twinning and fracturing. These fault cores may now serve as localized barriers to fault-normal flow because they are so heavily mineralized and are associated with poorly-developed to absent damage zones. Experimental results show that in other rock types, fault cores with similar textures to Class B fault cores have an order of magnitude lower permeability than fault cores composed of cataclasites (Seront et al., 1998).

The developmental sequence of these hydrologic components can be incorporated into paleohydrologic models. Class B fault zones appear to represent a minor population of the total fault zone population, and they are not likely to have large aerial extent considering their minor average displacements. However, because the DOE Active Fracture Model presupposes that as many as 20% of fractures are transmissive in the unsaturated zone at Yucca Mountain, it is possible that Class B fault zones may have measurable impact on groundwater flow at the local or broader scale. Class A and C fault zones developed sequentially, and as hydrologic components, they would cause increased fault-parallel permeability with increased fault-related strain. Faults with high displacement (associated with Class D fault zones) developed into

combined conduit-barrier systems acting to impede aquifer communication between blocks and enhance fault-parallel flow. Because each class of fault zone has a characteristic range of fault thickness and different architecture potentially leading to differences in permeability (Seront et al., 1998), fault zone classification may aid in assigning hydrologic properties to faults in groundwater flow models (e.g., Caine and Forster, 1999). Furthermore, the hydrologic properties of major faults are likely to change along a given fault plane as displacement varies, both along strike and up and down dip (Evans et al., 1997; Caine and Forster, 1999). Because faults lose displacement near the tip line of the fault, the clay-rich cores of Class D fault zones are likely to give way to the distributed conduit characteristics of Class C fault zones near the fault tip. A future slip event in a Class D fault zone could potentially change its hydrologic properties, however, this is unlikely within the next 10,000 years, because the recurrence rate of seismogenic faults at Yucca Mountain is 50,000 years or longer (Stepp et al., 2000). Although the detailed architecture of the fault zones we studied at Yucca Mountain are expected to influence the movement of groundwater, only direct measurements would be able to conclusively demonstrate effects of this kind.

5. Conclusions

Detailed examination of fault zones exposed in the ESF and ECRB of Yucca Mountain reveals four architectural classes. Three of these fault zone classes (Class A, C, and D) may represent a continuum of fault deformation related to increasing displacement and associated mechanical response of the welded tuffs. Faulting initiated along joints or fractures as discrete shears (Class A) is followed by progressive cataclasis (Class C), eventually leading to the development of a foliated gouge core and intensely fractured damage zone (Class D).

The fourth class of fault zones at Yucca Mountain (Class B) represents an unusual faulting style in which faults of generally minor displacement are heavily mineralized with blocky calcite during the period of fault activity. Continued displacement after fault rupture was accommodated by crystal plastic deformation and transcrystalline fracture and sliding of the

calcite and by discrete sliding along the core/damage zone boundaries. Class B fault zones are particularly significant because they constitute a secondary mineral occurrence that appears to be distinctly different from secondary mineralization found in lithophysae and fractures. In particular, they contain textures indicative of calcite mineralization in a fluid-saturated environment and deformation at elevated ($>170^{\circ}\text{C}$) temperatures. The age and origin of faults containing the Class B fault zones is unknown. Most fault-related strain in the region was accumulated soon after the tuffs were deposited approximately 11–12 Ma. At present, this lack of age control (relative or absolute) limits our ability to interpret their origin within existing tectonic-thermal and paleohydrologic models.

The diversity of fault zone architecture found in Yucca Mountain is important to paleohydrology and present-day hydrologic framework of Yucca Mountain and may be applicable to welded ignimbrites elsewhere. Class D fault zones have architecture that is conducive to fault parallel flow and impedes fault-normal flow. The hydrologic properties of smaller displacement faults within blocks should not be overgeneralized. Three distinct architectures exist with potentially different hydrologic properties ranging from discrete (Class A) to distributed conduits (Class C) and localized barriers (Class B). These three fault classes may be laterally gradational on high displacement faults and may produce lateral variations in the hydrologic properties of faults.

Acknowledgements

We thank Jonathan Caine, Tom Blenkinsop, Philip Justus, Bret Leslie, Hans Arlt, James Rubenstone, John Bradbury, Neil Coleman, Alan Morris, Brad Jordan, and Budhi Sagar for providing helpful review comments on this manuscript and Deborah Waiting and Brad Jordan for assistance with figure preparation. Brad Jordan assisted with the collection of the X-ray diffraction data. This paper was prepared to document work performed by the Center for Nuclear Waste Regulatory Analyses (CNWRA) for the U.S. Nuclear Regulatory Commission (NRC) under contract No. NRC-02-02-012. The studies and analyses reported here were performed on behalf of the NRC Office of Nuclear Material Safety and Safeguards, Division of

Waste Management. The report is an independent product of the CNWRA and does not necessarily reflect the views or regulatory position of the NRC.

Appendix A. Calcite twin analyses

A.1. Methodology

We used the calcite strain gauge technique (Groshong 1972, 1974; Evans and Groshong, 1994) to calculate calcite twinning strains in calcite grains from two mutually perpendicular thin sections from each sample. For each twin set measured, the average twin width, number of twins, grain width normal to twins, and the orientations of the c-axis and the e-twin plane were measured using a U-stage (Evans and Groshong, 1994). Widths of thin and thick twins were measured separately. The black line that constitutes a thin twin in an optical microscope includes a combination of twinned material and the optical effects of the twin boundaries. Using measured and calculated strains from experimentally deformed twinned calcite in limestone, Groshong (1974) determined that approximately 50% of the black line width represents twinned calcite (also see Groshong et al., 1984b). Typically, approximately 50 twin sets were measured from two perpendicular thin sections per sample. The principal strains (e_1 , e_2 , and e_3 expressed in % as + or - changes in length) and their orientations were calculated and output with the values of negative expected value (twin sets with sense of shear inconsistent with calculated strain tensor) and error. Cleaning was performed by removing of some portion, typically 20%, of twin sets with largest deviations from ideal orientations (often referred to as “largest deviations removed” or LDR). The square root of the second invariant of strain ($\sqrt{J_2}$ %) is used as a measure of the total distortion by twinning (Jaeger and Cook, 1979). J_2 is calculated from the three principal strains as follows: $J_2 = -(e_2e_3 + e_3e_1 + e_1e_2)$, where e_1 , e_2 , and e_3 are expressed as percent elongation.

The “mean twin width” for a sample was determined (following the approach of Ferrill, 1991) by first calculating the average twin width for each twin set (twin-set average) and then averaging the twin-set averages for the sample. Each twin-set average was calculated by summing the width of twinned material in a twin set, including both thick and thin twins, and dividing this by the total number of twins in the set. The standard twin-width sample average only includes twin sets used in the final twin-strain calculation and does not include sets removed during cleaning.

The twin intensity (twin planes/mm) for each twin set was calculated (following the approach of Ferrill, 1991) by dividing the number of twins in a set (including both thick and thin twins) by the width of the host grain (to the nearest micron) measured perpendicular to the twins. The “mean twin intensity” for a sample was calculated by averaging the twin-set averages for all twin sets measured in the sample. As with the twin width data, the mean twin intensity values only include twin sets used in the final twin-strain calculation.

In the Yucca Mountain rock samples, 28, 45, and 49, twin sets were measured in the three

samples (Table A1). Following the standard cleaning procedure, we discarded the 20% of measurements with the largest deviations. Twin thickness was measured using an eyepiece micrometer calibrated to a stage micrometer. Unless visibly thicker, thin twins were estimated to be 0.5 μm (microns) thick, with one half of that thickness (0.25 μm) twinned material. Each of the 965 twins larger than 0.5 μm (thick twins) was measured individually, and the histogram distribution of twin thicknesses for each sample is presented in Figure A1.

A.2. Results

Only three samples from fault zones in the Miocene volcanic tuffs at Yucca Mountain yielded a sufficient number of twinned calcite grains to perform a strain analysis. Total strain accommodated by twinning in the three samples was low, with values of 1.75, 0.29, and 2.09% (Table A1). Of the three samples, only sample SPC00530198 was oriented, and it featured a minimum extension direction approximately N-S and horizontal (Fig. 6a). The remaining two samples (02016200 and 02016201) were only oriented with respect to vertical and not with respect to north. However, in sample 02016200, the minimum extension direction was near the periphery of the stereonet (Fig. 6b), similar to sample SPC00530198, indicating a subhorizontal shortening. The maximum extension axis for sample 02016201 was located near the periphery of the stereonet as in the other two samples, but the minimum extension axis had a greater inclination than in the other samples. Based on the low strain in this sample, and the low relative difference between the minimum and intermediate extension values, such angular differences from other samples was to be expected. However, Figure 6 shows that the contoured minimum extension was close to the periphery of the stereonet.

References

- Allan, U.S., 1989. Model for hydrocarbon migration and entrapment within faulted structures. *American Association of Petroleum Geologists Bulletin* 73, 803–811.
- Beach, D.K., 1995. Controls and effects of subaerial exposure on cementation and development of secondary porosity in the subsurface of Great Bahama Bank. In: Budd, D.A., Saller, A.H., Harris, P.M. (Eds.), “Unconformities and Porosity in Carbonate Strata” *American Association for Petroleum Geologists Memoir* 63, pp. 1–34.
- Bredehoeft, J.D., 1997. Fault permeability near Yucca Mountain. *Water Resources Research* 33, 2459–2463.
- Brikowski, T., 1997. Fault-controlled vertical leakage inferred from water-table temperature variations at Yucca Mountain. Nuclear Waste Projects Office Technical Report 025-97, State of Nevada Agency for Nuclear Projects.
- Burkhard, M., 1993. Calcite twins, their geometry, appearance, and significance as stress-strain markers and indicators of tectonic regime: A review. *Journal of Structural Geology* 15, 351–368.
- Caine, J.S., Forster, C.B., 1999. Fault zone architecture and fluid flow: Insights from field data and numerical modeling. In: Haneberg, W.C., Mozley, P.S., Moore, J.C., Goodwin, L.B. (Eds.), *Faults and Subsurface Fluid Flow in the Shallow Crust*. Geophysical Monograph 113, pp. 101–127.
- Caine, J.S., Evans, J.P., Forster, C.B., 1996. Fault zone architecture and permeability structure. *Geology* 24, 1025–1028.
- Carter, N.L., Releigh, C.B., 1969. Principal stress directions from plastic flow in crystals. *Bulletin of the Geological Society of America* 80, 1231–1264.
- Chafetz, H.S., Wilkinson, B.H., Love, K.M., 1985. Morphology and composition of nonmarine carbonate cements in near-surface settings. In: Schneidermann, N., and Harris, P.M. (Eds.), *Carbonate Cements*. S.E.P.M. Special Publication 36, pp. 337–347.
- Chester F.M., Logan, J.M., 1987. Composite planar fabric of gouge from the Punchbowl Fault, California. *Journal of Structural Geology* 9, 621–634.
- Cladouhos, T.T., 1999. A kinematic model for deformation within brittle shear zones. *Journal of Structural Geology* 21, 437–448.
- Cline, J.S., Wilson, N.S.F., 2001. Paragenesis of secondary mineralization at Yucca Mountain, Nevada, U.S.A. In: Cidu, R. (Ed.), *Water-Rock Interaction 2001*. Proceedings of the Tenth International Symposium on Water-Rock Interaction, Balkema, The Netherlands, pp. 1311–1314.
- CRWMS M&O (Civilian Radioactive Waste Management System Management and Operating Contractor), 1997. Yucca Mountain site geotechnical report. B00000000-01717-5705-00043 REV 01. Las Vegas, Nevada: CRWMS M&O.
- CRWMS M&O (Civilian Radioactive Waste Management System Management and Operating Contractor), 1998. Geology of the Exploratory Studies Facility Topopah Spring Loop. BAB000000-01717-0200-00002, REV 01. U.S. Department of Energy, Las Vegas, Nevada.

- Day, W.C., Dickerson, R.P., Potter, C.J., Sweetkind, D.S., San Juan, C.A., Drake, R.M., II, Fridrich, C.J., 1998. Bedrock geologic map of the Yucca Mountain area, Nye County, Nevada. U.S. Geological Survey Map I-2627, scale 1:24,000.
- Dublyansky, Y., Szymanski, J., Chepizhko, A., Lapin, B., Reutski, V., 1998. Geological history of Yucca Mountain (Nevada) and the problem of a high-level nuclear waste repository. In: Stenhouse, M.J., Kirko, V.I. (Eds.), *Defence Nuclear Waste Disposal in Russia*. NATO Series Kluwer Academic Publishing, Netherlands, pp. 279–292.
- Dublyansky, Y., Ford, D., Reutski, V., 2001. Traces of epigenetic hydrothermal activity at Yucca Mountain, Nevada; preliminary data on the fluid inclusion and stable isotope evidence. *Chemical Geology* 173, 125–149.
- Eatman, G.L.W., Singleton, W.L., Moyer, T.C., Barr, D.L., Albin, A.L., Lung, R.C., Beason, S.C., 1997. Geology of the South Ramp Station 55+00 to 78+77, Exploratory Studies Facility, Yucca Mountain Project, Yucca Mountain, Nevada. Department of Energy Report, DTN GS96090831224.020.
- Eichhubl, P., Boles, J.R., 2000. Focused fluid flow along faults in the Monterey Formation, coastal California. *Geological Society of America Bulletin* 112, 1667–1679.
- Evans, J.P., 1990. Thickness-displacement relationships for fault zones. *Journal of Structural Geology* 12, 1061–1065.
- Evans, M.A., Dunne, W.M., 1991. Strain factorization and partitioning in the North Mountain thrust sheet, central Appalachians, U.S.A. *Journal of Structural Geology* 13, 21–35.
- Evans, M.A., Groshong, R.H., Jr., 1994. A computer program for the calcite strain gauge technique. *Journal of Structural Geology* 16, 277–281.
- Evans, J.P., Bradbury, K.K., 2004. Faulting and fracturing of nonwelded Bishop Tuff, Eastern California: Deformation mechanisms in very porous materials in the vadose zone. *Vadose Zone Journal* 3, 602–623.
- Evans, J.P., Forster, C.B., Goddard, J.V., 1997. Permeability of fault-related rocks, and implications for hydraulic structure of fault zones. *Journal of Structural Geology* 19, 1393–1404.
- Ferrill, D.A., 1991. Calcite twin widths and intensities as metamorphic indicators in natural low-temperature deformation of limestone. *Journal of Structural Geology* 13, 667–675.
- Ferrill, D.A., 1998. Critical re-evaluation of differential stress estimates from calcite twins in coarse-grained limestone. *Tectonophysics* 285, 77–86.
- Ferrill, D.A., Groshong, R.H., Jr., 1993. Deformation conditions in the northern Subalpine Chain, France, estimated from deformation modes in coarse-grained limestone. *Journal of Structural Geology* 15, 995–1006.
- Ferrill, D.A., Morris, A.P., 2003. Dilational normal faults. *Journal of Structural Geology* 25, 183–196.
- Ferrill, D.A., Stirewalt, G.L., Henderson, D.B., Stamatakos, J.A., Morris, A.P., Spivey, K.H., Wernicke, B.P., 1995. Faulting in the Yucca Mountain Region. Critical review and analysis of tectonic data from the Central Basin and Range. NUREG/CR-6401. CNWRA 95-017. Center for Nuclear Waste Regulatory Analyses, San Antonio, Texas.
- Ferrill, D.A., Winterle, J., Wittmeyer, G., Sims, D.W., Colton, S., Armstrong, A., Morris, A.P.,

1999. Stressed rock strains groundwater at Yucca Mountain, Nevada. *Geological Society of America Today* 9, 1–8.
- Ferrill, D.A., Morris, A.P., Stamatakos, J.A., Sims, D.W., 2000. Crossing Conjugate Normal Faults. *American Association of Petroleum Geologists Bulletin* 84, 1543–1559.
- Ferrill, D.A., Morris, A.P., Evans, M.A., Burkhard, M., Groshong, R.H., Onasch, C. M., 2004. Calcite twin morphology: A low-temperature deformation geothermometer. *Journal of Structural Geology* 26, 1521-1529.
- Finkbeiner, T., Barton, C.A., Zoback, M.D., 1997. Relationships among in-situ stress, fractures and faults, and fluid flow: Monterey Formation, Santa Maria Basin, California. *American Association of Petroleum Geologists Bulletin* 81, 1975–1999.
- Fleuty, M.J., Weaver, J.D, 1975. Slickensides and slickenlines. *Geological Magazine* 112, 319–322.
- Flügel, E., 1982. *Microfacies analysis of limestones*. Springer-Verlag, New York.
- Folk, R.L., 1974. The natural history of crystalline calcium carbonate: Effect of magnesium content and salinity. *Journal of Sedimentary Petrology* 44, 40–53.
- Fridrich, C.J., Whitney, J.W., Hudson, M.R., Crowe, B.M., 1999. Late Cenozoic extension, vertical axis rotation, and volcanism in Crater Flat basin, southwest Nevada. In: Wright, L., Troxel, B. (Eds.), *Cenozoic Basins of the Death Valley Region*. Geological Society of America Special Paper 333, pp. 197–212.
- Friedman, G.M., 1965. Terminology of crystallization textures and fabrics in sedimentary rocks. *Journal of Sedimentary Petrology* 35, 643–655.
- Frizzell, V.A., Schulters, J., 1990. Geologic map of the Nevada Test Site, southern Nevada. U.S. Geological Survey Map I-2046, scale 1:100,000.
- Goddard, J.V., Evans, J.P., 1995. Fluid-rock interactions in faults of crystalline thrust sheets, northwestern Wyoming, U.S.A. Inferences from geochemistry of fault-related rocks. *Journal of Structural Geology* 17, 533–549.
- Gray, M.B., Stamatakos, J.A., Ferrill, D.A., 2000. Polygenetic secondary calcite mineralization in Yucca Mountain, NV. *Geological Society of America Abstracts with Programs* 32, A-260
- Gray, M.B., Stamatakos, J.A., Ferrill, D.A., Evans, M.,A. 1999. Fault behavior and fault zone architecture in Miocene tuffs at Yucca Mountain. *EOS, Transactions of the American Geophysical Union* 80 (46), 741.
- Gray, M.B., Stamatakos, J.A., Ferrill, D. A., 1998. Microstructural and microtextural analyses of faulting at Yucca Mountain, Nevada, *EOS, Transactions of the American Geophysical Union*. 79, (45) F823.
- Groshong, R.H., Jr., 1972. Strain calculated from twinning in calcite. *Bulletin of the Geological Society of America* 82, 2025–2038.
- Groshong, R.H., Jr., 1974. Experimental test of least-squares strain gage calculation using twinned calcite. *Bulletin of the Geological Society of America* 58, 1855–1864.
- Groshong, R.H., Jr. 1988. Low-temperature deformation mechanisms and their interpretation. *Bulletin of the Geological Society of America* 100, 1329–1360.
- Groshong, R.H., Jr., Pfiffner, O.A., Pringle, L.R., 1984a. Strain partitioning in the Helvetic thrust

- belt of eastern Switzerland from the leading edge to the internal zone. *Journal of Structural Geology* 6, 5–18.
- Groshong, R.H., Jr., Teufel, L.W., Gasteiger, C., 1984b. Precision and accuracy of the calcite strain-gage technique. *Bulletin of the Geological Society of America* 95, 357–363.
- Hill, C.A., Dublyansky, Y.V., Harmon, R.S., Schluter, C.M., 1995. Overview of calcite/opal deposits at or near the proposed high-level nuclear waste site, Yucca Mountain, Nevada, USA; pedogenic, hypogene, or both? *Environmental Geology* 26, 69–88.
- Hull, J., 1988. Thickness-displacement relationships for deformation zones. *Journal of Structural Geology* 10, 431–435.
- Jaeger, J.C., Cook, N.G.W., 1979. *Fundamentals of Rock Mechanics*, 3rd ed, Chapman and Hall, London.
- Kim Y-S., Peacock, D.C.P., Sanderson, D.J., 2003. Mesoscale strike-slip faults and damage zones at Marsalforn, Gozo Island, Malta. *Journal of Structural Geology* 25, 793–812.
- Knott, S.D., 1994. Fault zone thickness versus displacement in the Permo-Triassic sandstones of NW England. *Journal of the Geological Society of London* 151, 17–25.
- Land, L.S., 1970. Phreatic versus vadose meteoric diagenesis of limestones: Evidence from a fossil water table. *Sedimentology* 14, 175–185.
- Levy, S., Chippera, S., WoldeGabriel, G., Fabryka-Martin, J., Roach, J., Sweetkind, D.S., 1999. Flow-path textures and mineralogy in tuffs of the unsaturated zone. In: Haneberg, W.C., Mozley, P.S., Moore, J.C., Goodwin, L.B. (Eds.), *Faults and Subsurface Fluid Flow in the Shallow Crust*. Geophysical Monograph 113, pp. 159–184.
- Mongano, G.S., Singleton, W.L., Moyer, T.C., Beason, S.C., Eatman, G.L.W., Algin, A.L., Lung, R.C., 1999. *Geology of the ECRB Cross Drift Exploratory Studies Facility, Yucca Mountain Project, Yucca Mountain, Nevada*.
http://www.ymp.gov/timeline/site/spg2gm3_a/
- Moore, D.M., Reynolds, R.C., 1989. *X-ray diffraction and the identification and analysis of clay minerals*. Oxford University Press, Oxford.
- Muchez, P., Sintubin, M., 1998. Contrasting origin of paleofluids in a strike-slip fault system. *Chemical Geology* 145, 105–114.
- National Academy of Sciences, 1992. *Groundwater at Yucca Mountain - How high can it rise? Final Report of the Panel on Coupled Hydrologic/Tectonic/Hydrothermal Systems at Yucca Mountain*. National Academy Press. Washington, D.C.
- Neymark, L.A., Paces, J.B., 2000. Consequences of slow growth for ²³⁰Th/U dating of Quaternary opals, Yucca Mountain, NV, USA. *Chemical Geology* 164, 143–160.
- Neymark, L.A., Amelin, Y., Paces, J.B., Peterman, Z., 2002. U-Pb ages of secondary silica at Yucca Mountain, Nevada: implications for the paleohydrology of the unsaturated zone. *Applied Geochemistry* 17, 709–734.
- Ofoegbu, G.I., Painter, S., Chen, R., Fedors, R.W., Ferrill, D.A., 2001. Geomechanical and thermal effects on moisture flow at the proposed Yucca Mountain nuclear waste repository. *Nuclear Technology* 134, 241–262.
- Paces, J.B., Neymark, L.A., Marshall, B.D., Whelan, J.F., Peterman, Z.E., 2001. Ages and origins of calcite and opal in the Exploratory Studies Facility Tunnel, Yucca Mountain,

- Nevada. U.S. Geological Survey Water Resources Investigation Report 01-4049. 95 p.
- Painter, S., Winterle, J., 2003. Using temperature to test models of flow near Yucca Mountain, Nevada. *Ground Water* 41, 657-666.
- Passchier, C.W., Simpson, C., 1986. Porphyroclast systems as kinematic indicators. *Journal of Structural Geology* 8, 831-843.
- Philips, Inc., 1999a. PC-APD (personal computer-automated powder diffraction) software. Part #PW1877, version 3.6J, October 1, 1999, Y2K compliant, Copyright Philips Electronics, N.V. 1999 All rights reserved.
- Philips, Inc., 1999b. PW1876 PC-IDENTIFY software. Version 1.0J, September 9, 1999, Y2K compliant, Copyright Philips Electronics, N.V. 1999 All rights reserved.
- Potter, C.J., Day, W.C., Sweetkind, D.S., Dickerson, R.P., 2004. Structural geology of the proposed site area for a high-level radioactive waste repository, Yucca Mountain, Nevada. *Geological Society of America Bulletin* 116, 858-879.
- Ramsey, J.M., Chester, F.M., 2004. Hybrid fracture and the transition from extension fracture to shear fracture. *Nature* 428, 63-66.
- Rogers, A.M., Harmsen, S.C., Corbett, E.J., Priestly, K., DePolo, D., 1991. The seismicity of Nevada and some adjacent parts of the Great Basin. In: Slemmons, D.B., Engdahl, E.R., Zoback, M.D., Blackwell, D.D. (Eds.), *Neotectonics of North America*. Geological Society of America, Denver, CO, pp. 153-184.
- Rowling, G., Goodwin, L., Wilson, J., 2001. Internal architecture, permeability structure, and hydrologic significance of contrasting fault zone types. *Geology* 29, 43-46.
- Rutter, E.H., Maddock, R.H., Hall, S.H., White, S.H., 1986. Comparative microstructures of natural and experimentally produced clay-bearing fault gouges. *Pure and Applied Geophysics* 124, 3-30.
- Sawyer, D.A., Fleck, R.J., Lanphere, M.A., Warren, R.G., Broxton, D.E., Hudson, M.R., 1994. Episodic caldera volcanism in the Miocene southwestern Nevada volcanic field: revised stratigraphic framework, $^{40}\text{Ar}/^{39}\text{Ar}$ geochronology, and implications for magmatism and extension. *Geological Society of America Bulletin* 106, 304-1318.
- Scholle, P.A., Ulmer-Scholle, D.A., 2003. A color guide to the petrography of carbonate rocks: grains textures, porosity, diagenesis. *American Associations of Petroleum Geologists Memoir 77*, American Association of Petroleum Geologists, Tulsa, Oklahoma.
- Seront, B., Wong, T.-F., Caine, J.S., Forster, C.B., Bruhn, R.H., Fridrich, J.T., 1998. Laboratory characterization of hydromechanical properties of a seismogenic normal fault system. *Journal of Structural Geology* 20, 865-881.
- Sibson, R.H., 1977. Fault rocks and fault mechanisms. *Journal of the Geological Society* 133, 191-213.
- Sibson, R.H., 1986. Brecciation processes in fault zones: Inferences from earthquake rupturing. *Pure and Applied Geophysics* 124, 159-175.
- Sibson, R.H., 1994. Crustal stress, faulting and fluid flow. In: Parnell, J. (Ed.), *Geofluids: Origin, Migration, and Evolution of Fluids in Sedimentary Basins*. Geological Society Special Publication 78, pp. 69-84.
- Smart, K.J., Dunne W.M., Krieg, R.D., 1997. Roof sequence response to emplacement of the

- Wills Mountain duplex: the roles of forethrusting and scales of deformation. *Journal of Structural Geology* 19, 1443–1459.
- Spengler, R. W., Byers, F.M., Jr., Warner, J.B., 1981. Stratigraphy and structure of volcanic rocks in Drill Hole Wash USW G-1, Yucca Mountain, Nye County, Nevada. U.S. Geological Survey Open File Report 81-1349.
- Spraggins, S.A., Dunne, W.M., 2002. Deformation history of the Roanoke recess, Appalachians, USA. *Journal of Structural Geology* 24, 411–433.
- Starkey, H.C., Blackmon, P.D., Hauff, P.L., 1984. The routine mineralogical analysis of clay-bearing samples. U.S. Geological Survey Bulletin B, p. 1563.
- Stepp, J.C., Wong, I., Whitney, J., Quittmeyer, R., Abrahamson, N., Toro, G., Youngs, R., Coppersmith, K., Savy, J., Sullivan, T., Yucca Mountain PSHA Project Members, 2000. Probabilistic Seismic Hazard Analyses for Ground Motions and Fault Displacements at Yucca Mountain, Nevada. *Earthquake Spectra* 17, 113–151.
- Stuckless, J.S., Peterman, Z.E., Forester, R.M., Whelan, J.F., Vaniman, D.T., Marshall, B.D., Taylor, E.M., 1992. Characterization of fault-filling deposits in the vicinity of Yucca Mountain, Nevada. Waste Management 1992 Conference Proceedings, Tucson, AZ, Waste Management, 929–935.
- Stuckless, J.S., Marshall, B.D., Vaniman, D.T., Dudley, W.W., Peterman, Z.E., Paces, J.B., Whelan, J.F., Taylor, E.M., Forester, R.M., O'Leary, D.W., 1998. Overview of calcite/opal deposits at or near to the proposed high-level nuclear waste site, Yucca Mountain, Nevada, U.S.A.: Pedogenic, hypogene, or both?; discussion. *Environmental Geology* 34, 70–78.
- Sweetkind, D.S., Williams-Stroud, S.C., 1996. Characteristics of fractures at Yucca Mountain, Nevada: Synthesis report. U.S. Geologic Survey Administrative Report. Denver, CO: U.S. Geological Survey.
- Tucker, M.E., Wright, V.P., 1990. Carbonate Sedimentology. Blackwell Scientific Publications. Oxford.
- Turner, F.J., 1953. Nature and dynamic interpretation of deformation lamellae in calcite of three marbles. *American Journal of Science* 251, 276–298.
- Whelan, J.F., Moscati, R.J., 1998. 9 M.Y. record of Southern Nevada climate from Yucca Mountain secondary minerals. Proceedings of the Eighth International Conference on High-Level Radioactive Waste Management, pp. 12–15.
- Whelan, J.F., Paces, J.B., Peterman, Z.E., 2002. Physical and stable-isotope evidence for formation of secondary calcite and silica in the unsaturated zone, Yucca Mountain, Nevada. *Applied Geochemistry* 17, 735–750.
- Wilson, J.E., Goodwin, L.B., Lewis, C.J., 2003. Deformation bands in nonwelded ignimbrites: Petrophysical controls on fault-zone deformation and evidence of preferential fluid flow. *Geology* 31, 837-840.
- Wilson, N.S.F., Cline, J.S., 2002. Thermochronological evolution of calcite: Formation at the proposed Yucca Mountain Repository Site, Nevada - Part 1, secondary mineral paragenesis and geochemistry. Report TR-02-005.1 Yucca Mountain Project, Department of Energy.
- Wilson, N.S.F., Cline, J.S., Amelin, Y.V., 2003. Origin, timing, and temperature of secondary calcite-silica mineral formation at Yucca Mountain, Nevada. *Geochimica et Cosmochimica*

Acta 67, 1145–1176.

Wojtal, S.F., Mitra, G., 1986. Strain hardening and strain softening in fault zones from foreland thrusts. *Geological Society of America Bulletin* 97, 674–687.

Zhang, X., Sanderson, D.J., 1996. Numerical modeling of the effects of fault slip on fluid flow around extensional faults. *Journal of Structural Geology* 18, 109–119.

Figure Captions

Figure 1. Location and geologic setting of a potential Yucca Mountain high-level radioactive waste repository within the Basin and Range physiographic province. Geology in (a) is from Frizzell and Schulters (1990) and Day et al. (1998). Digital elevation model in (b) is from the United States Geological Survey Digital Line Graph Data Set. Geologic cross section in (c) is from Ferrill et al. (1995).

Figure 2. (a) Geologic map and (b) cross section of Yucca Mountain showing the location of the Exploratory Studies Facility and Cross Drift relative to mapped faults. Map and cross section are modified from Day et al., (1998). Site coordinates are latitude-longitude and Nevada State Plane, in feet.

Figure 3. Illustration of the main features in cross section of the four main fault zones classes observed in the Exploratory Studies Facility and Cross Drift at Yucca Mountain, Nevada. Class A fault zones are discrete slickensided fractures with minor displacements and little or no damage zone. Class B fault zones have thin, mineralized brecciated cores and poorly developed damage zones. The boundaries between Class B cores and damage zones are slickensided. Class C fault zones are composed of well developed brecciated cores and intensely fractured damage zones. Class D fault zones have a composite core comprising foliated clay gouge and surrounding breccia. Class D damage zones are well developed and correspondingly thick. See text for further description of fault zone classes.

Figure 4. Fault width data for faults mapped in the Exploratory Studies Facility (ESF). The data are from the 112 fault zones identified in the data set that have recorded fault-zone widths. Fault data are from the EFS; (U.S. Department of Energy to the Center for Nuclear Waste Regulatory Analyses, August, 1998, U.S. Department of Energy Data Tracking Number numbers GS960708314224.008, .101, .011, .014, .003, .008, .010, .012, .020, .021, .022, .023, .024, .025, .026, and .028; Technical Data Information Form numbers 305556, 305554, 305624, 306645, 306017, 306284, 306298, 306299, 306509, 306510, 306511, 306512, 306513, 306514, 306515, 306516, 306517).

Figure 5. Photographs of the fault zones that represent the four fault classes at Yucca Mountain. (a) Class A fault zone exposed near Station 0+34 in Alcove 5 of the ESF. (b) Class B fault zone exposed near ESF Station 76+17.8. The heavily mineralized fault core has well-defined slickensided boundaries flanked by an intensely fractured, relatively narrow damage zone. Note the rock hammer for scale. (c) Class C thrust fault zone that crops out in Alcove 6, at Station 00+86. Note the rock chisel for scale. (d) Class D fault zone that crops out in the Cross Drift. The view is looking north at the Solitario Canyon fault core. The foliated smectitic gouge is surrounded by breccia with patchy opal/calcite mineralization and oxidized matrix.

Figure 6. Equal-area, lower-hemisphere projections showing the distribution of calculated

compression axes (small filled circles), contours of the compression axes in standard deviation (increments of 1, 2, 3, etc., standard deviations), and orientation of the axes of the calcite twin strain ellipsoid [solid square = minimum extension axis (e3), solid triangle is the intermediate extension axis (e2), and solid circle is the maximum extension axis (e1)]. ESF sample SPC00530198 at Station 43+39 (a) is precisely oriented and shows the orientation of the fault sampled. Principal strain axes for this sample are consistent with right-lateral strike-slip deformation in the calcite matrix. Core samples 02016200 and 02016201 (b and c) are from flow breccia in USW G-1 at depths of 1086.8–1087.1 and 1087.2–1087.3 m, respectively (Spengler et al., 1981). Core samples are not oriented with respect to north. North is somewhere on the periphery of the stereonet. Sample 02016200 in (b) shows principal strain axes that are also consistent with deformation in a strike-slip strain field, while principal strain axes for sample 02016201 in (c) imply a strain field that is transitional between extension and strike-slip.

Figure 7. Photomicrographs of features observed in the faulted tuffs. (a) Calcite matrix from a sample at ESF Station 43+39 (SPC00530198) that shows characteristic poikilotopic texture (cross-polarized light). Elongated wall rock clasts are opaque. Calcite strain gauge data collected from this fault are presented in Fig. 8a. (b) Calcite crystals (cross-polarized light) that contain intra- and intercrystalline fractures along which sliding has taken place. The sample is from Station 54+73.5 (SPC00552524). (c) Photomicrograph of slightly bent thick twins (dark bands in central crystal, white bands in upper right crystal) in sample SPC00530198. Thin twins are also visible in central crystal. (d) A postkinematic vein, shown in cross-polarized light, that transects strained calcite matrix in a sample from ESF Station 43+39 (SPC00530198). (e) Cataclasite within the Sundance fault (plane-polarized light), SPC00552529B (ESF Station 35+92.5). (f) Cataclasite within the Ghost Dance fault (plane-polarized light), SPC00534024A (Alcove 6), showing transgranular shear that offset a chalcedony vein. (g) Solitario Canyon fault gouge (SPC00543706B) with sigmoidal P-foliation is asymptotic into shear planes subparallel to shear zone boundary. Photomicrograph is plane-polarized light. Thin section is necessarily overly thick to avoid plucking during section preparation. Asymmetry is consistent with hanging wall down-to-the-west sense of shear.

Figure 8. Data on the effect of primary anisotropy on the orientation of the long axis of clasts and the clast bounding fractures in a Class B fault core (SPC00530198G at Station 43+39).. (a) and (b), respectively, and a Class C fault core from SPC 00552529B at ESF Station 35+92.5 (the Sundance Fault) (c) and (d), respectively. (a) Most clasts are elongated subperpendicular to the eutaxitic foliation, indicating that Class B fault zones did not undergo significant clast comminution and the faults were initiated by rupture at a high angle to layering. (b) Most clasts are bounded by fractures at high angles to the eutaxitic foliation. (c) Class C fault zones underwent more comminution than Class B fault zones resulting in more clasts with long axes subparallel to the eutaxitic foliation. (d) Fractures subparallel to the eutaxitic foliation (primary anisotropy) are most common, and other orientations are evenly distributed, indicating comminution of wall rock clasts by cataclastic flow. Data were gathered from thin sections cut parallel to transport direction and normal to the fault plane.

Figure 9. Calcite twin strain data replotted from Ferrill et al. (2004). The twin data from our Yucca Mountain sample is also shown as yellow stars.

Figure 10. Conceptual model of the genetic and spatial relationships between Class A, C and D fault zones. (a) Increasing displacement causes strain hardening of fault cores and fault core growth. Highest displacement faults (Class D) develop a zone of foliated gouge in their cores. (b) Fault displacement gradients are expected to correspond with spatial changes in fault zone architecture. See text for discussion.

Figure A1. Histograms showing the distribution of measured thick twin widths in the three samples studied. Note that sample SPC00530198 has a higher number of twins larger than 1 micron wide.

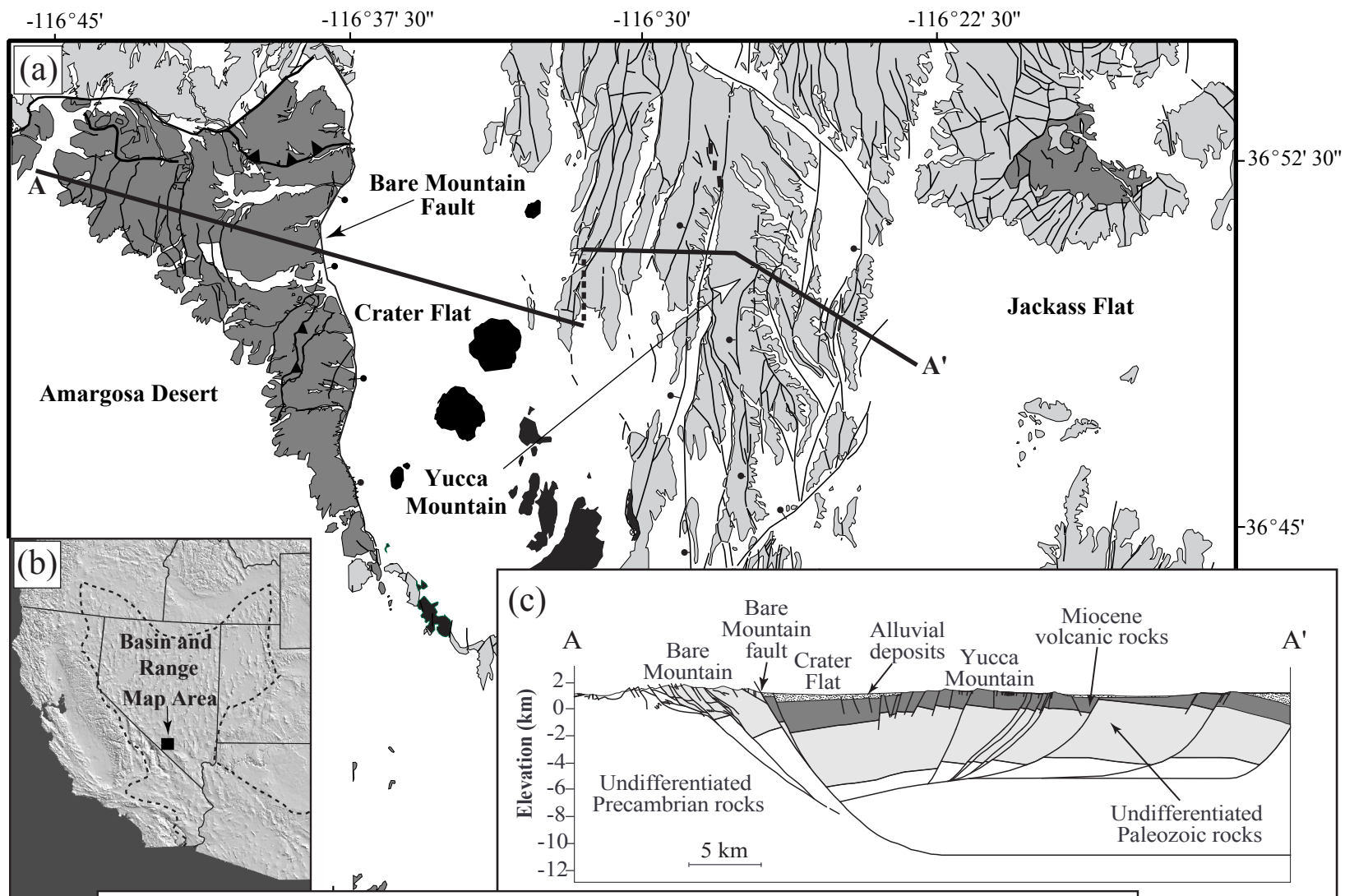


Figure 1
 Gray et al., 2004

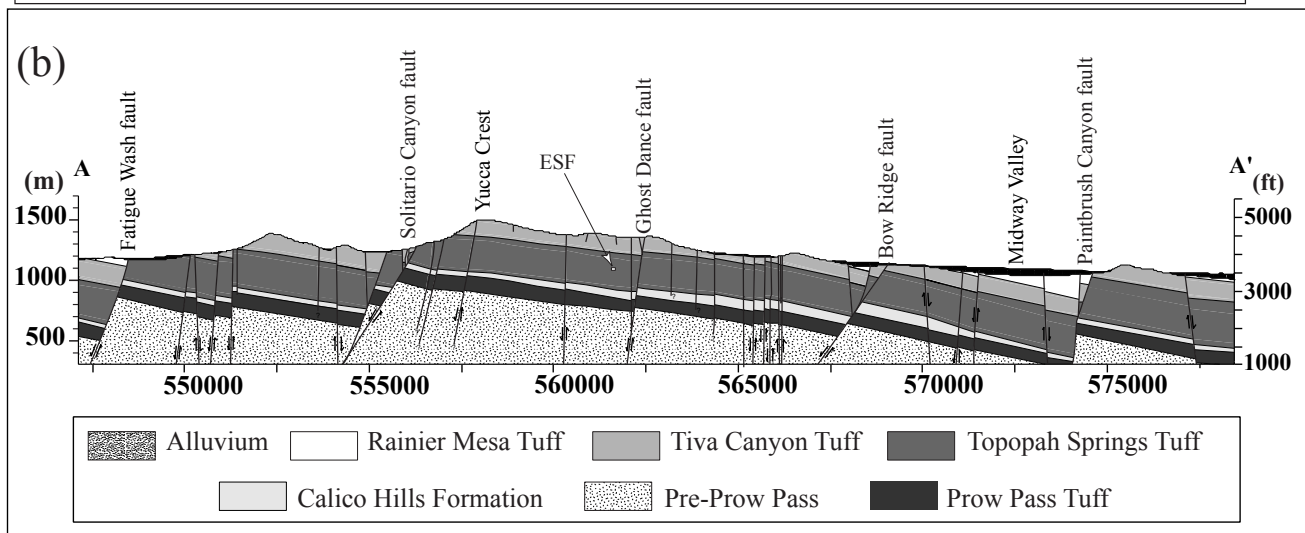
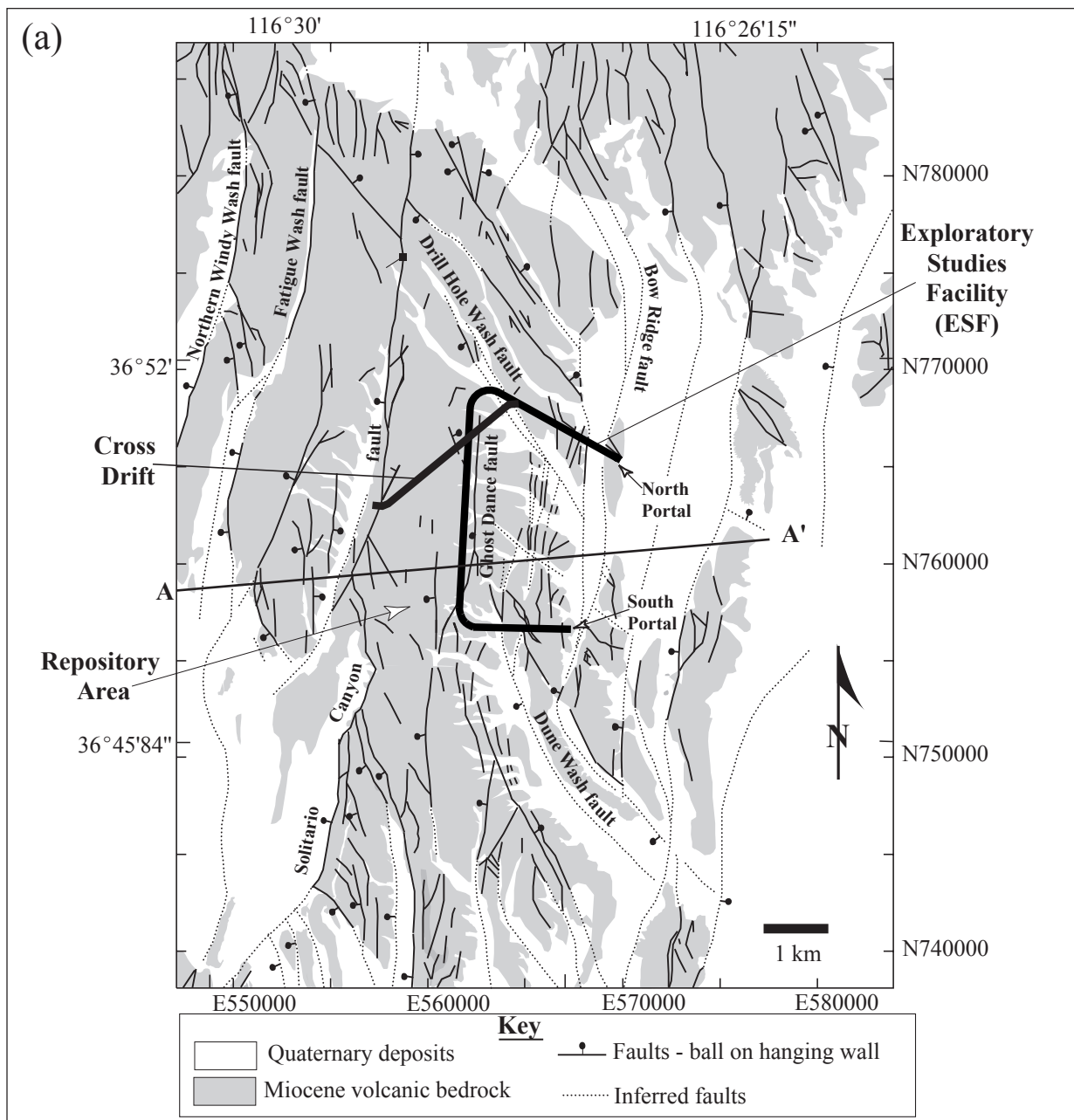


Figure 2
Gray et al., 2004

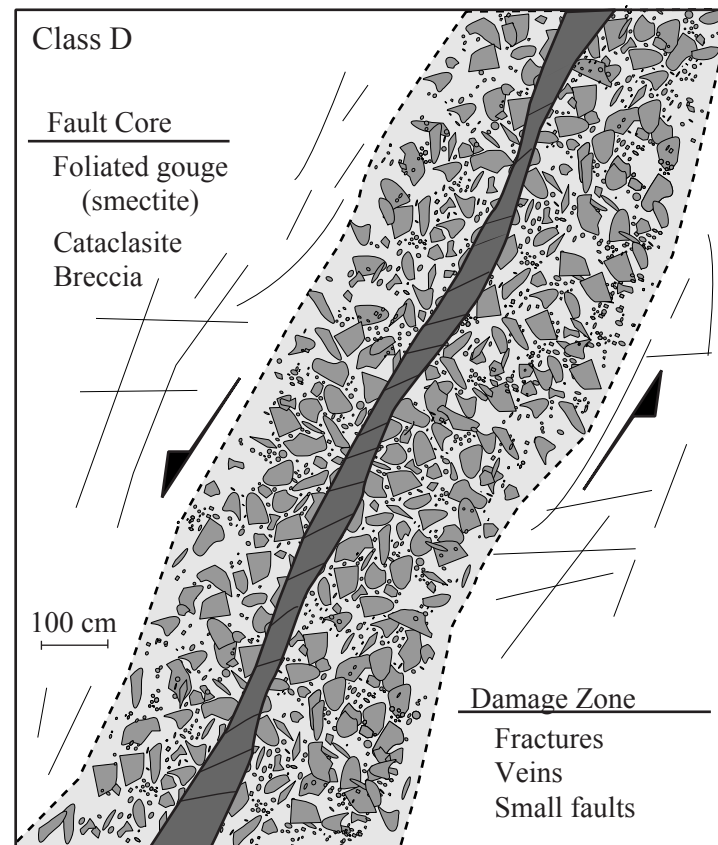
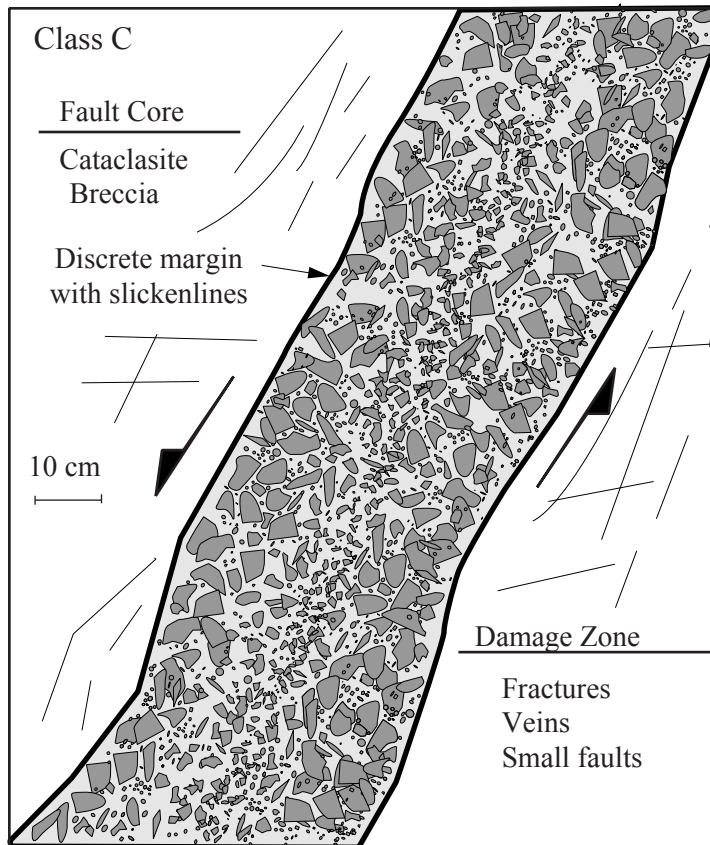
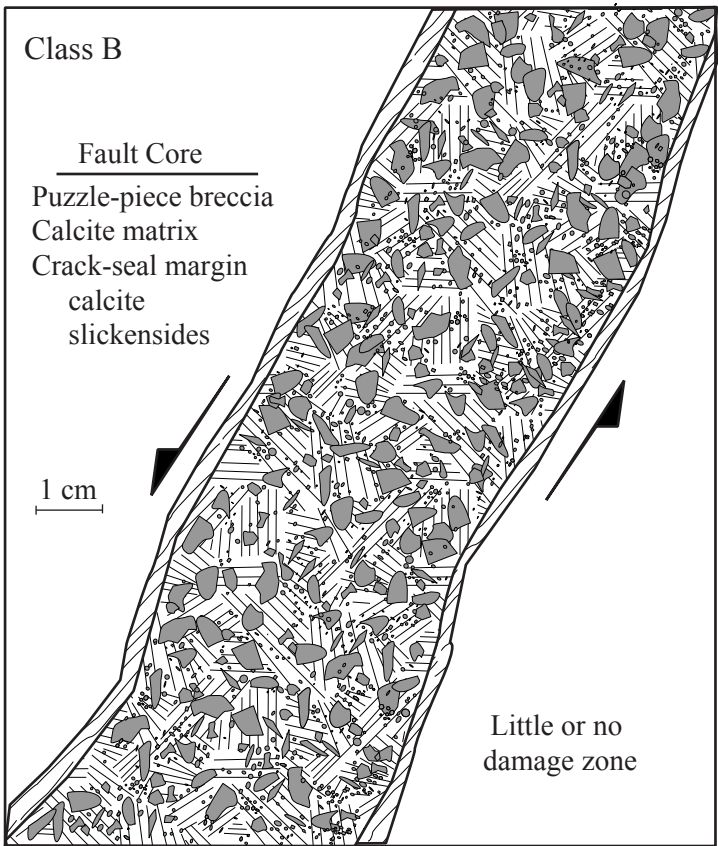
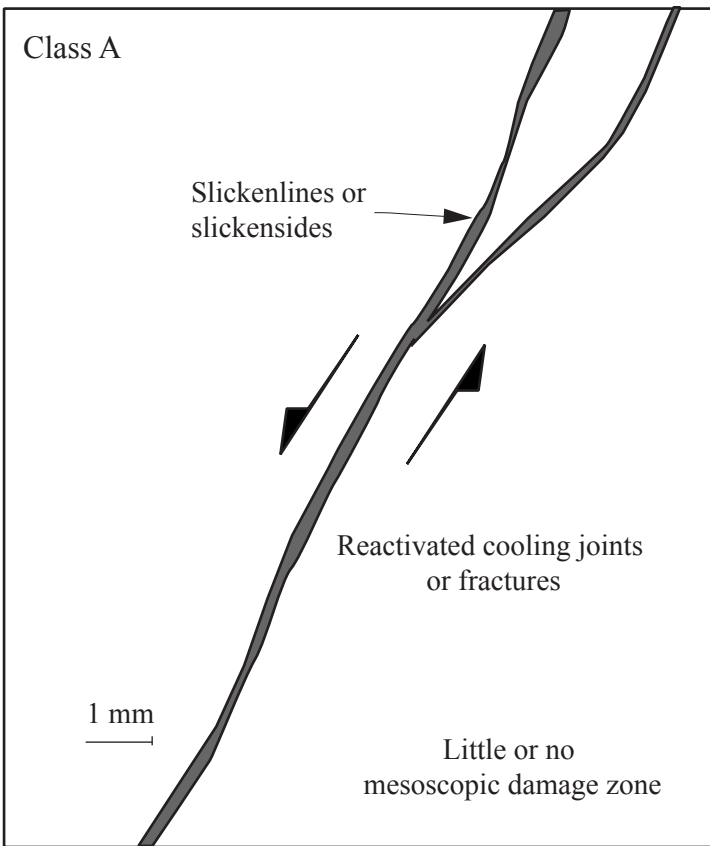


Figure 3
Gray et al., 2004

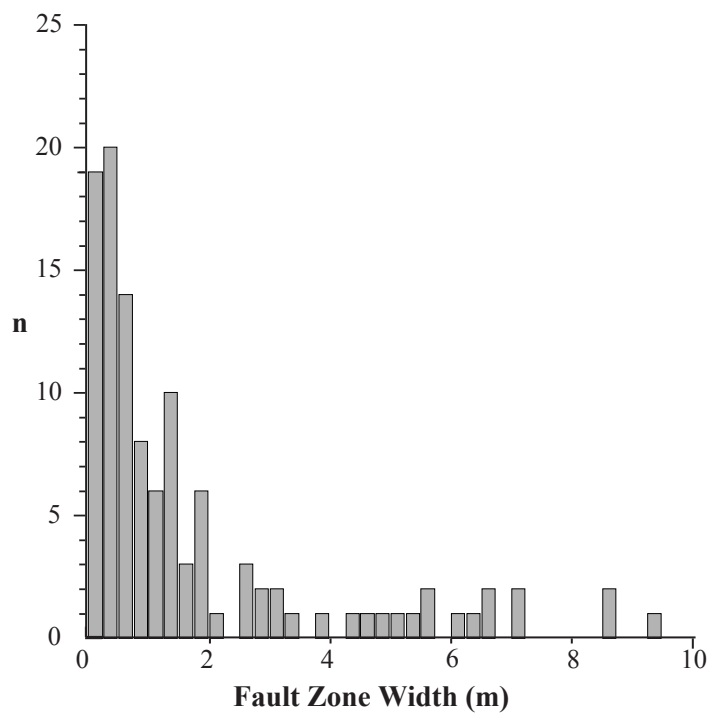


Figure 4
Gray et al., 2004

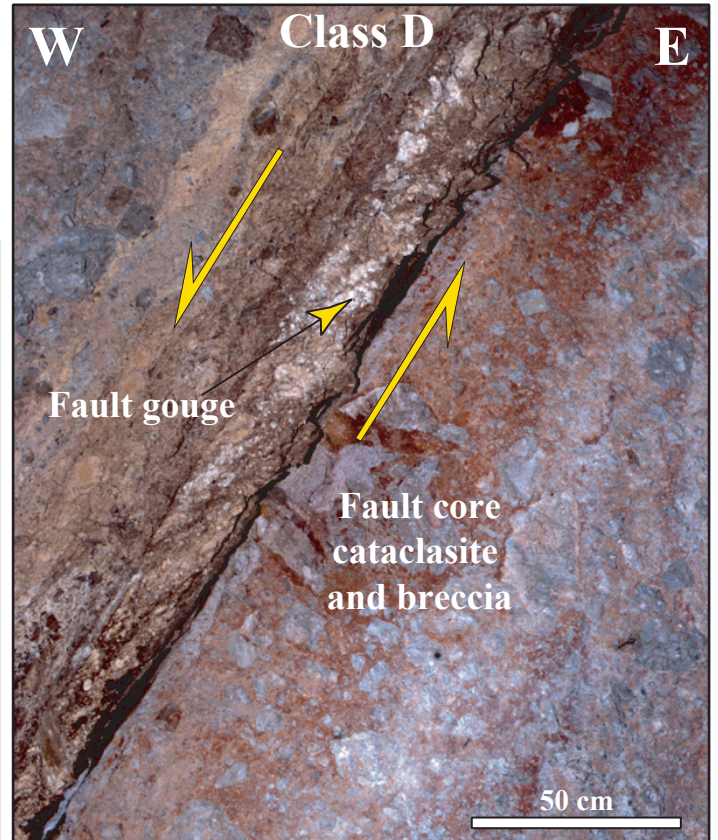
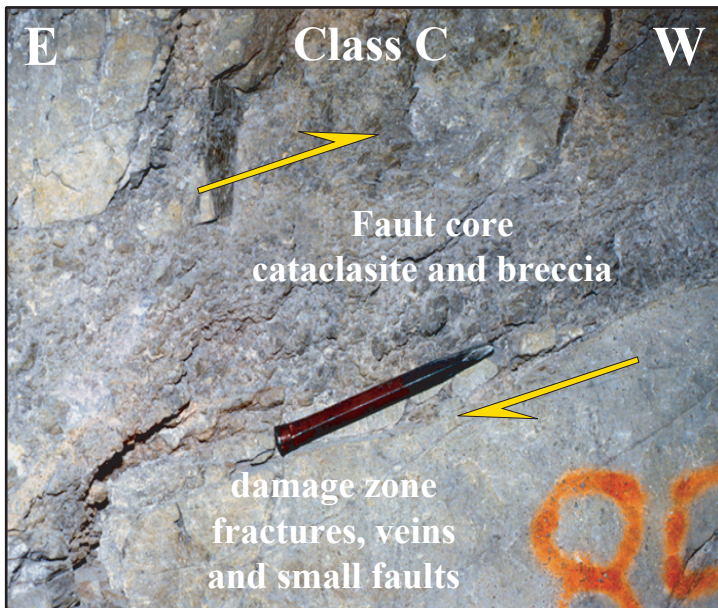
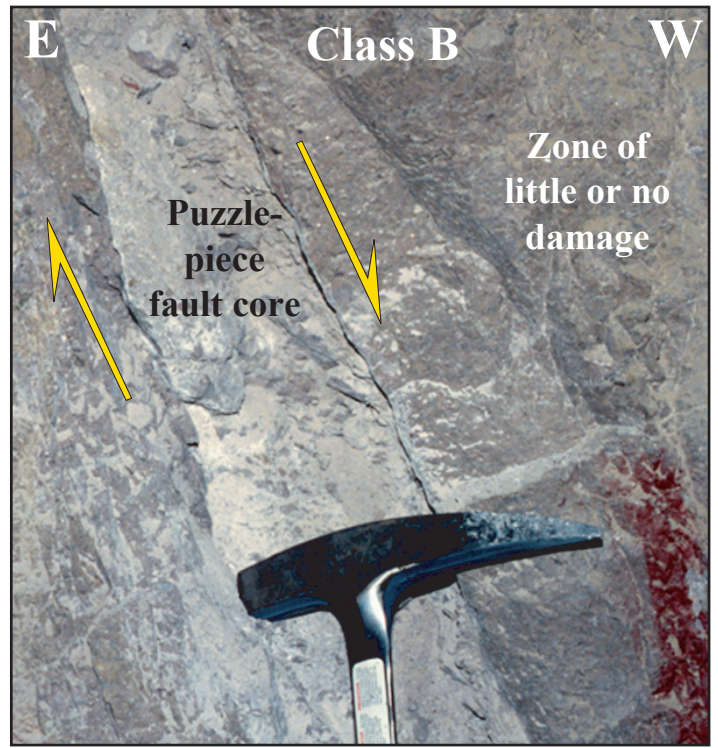
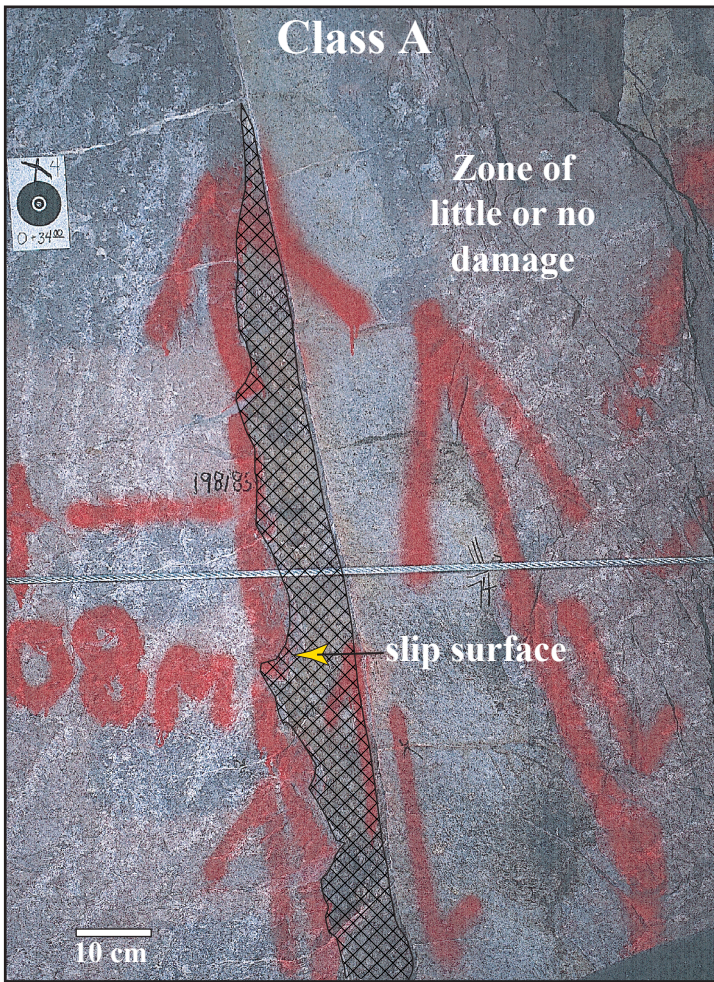


Figure 5
Gray et al., 2004

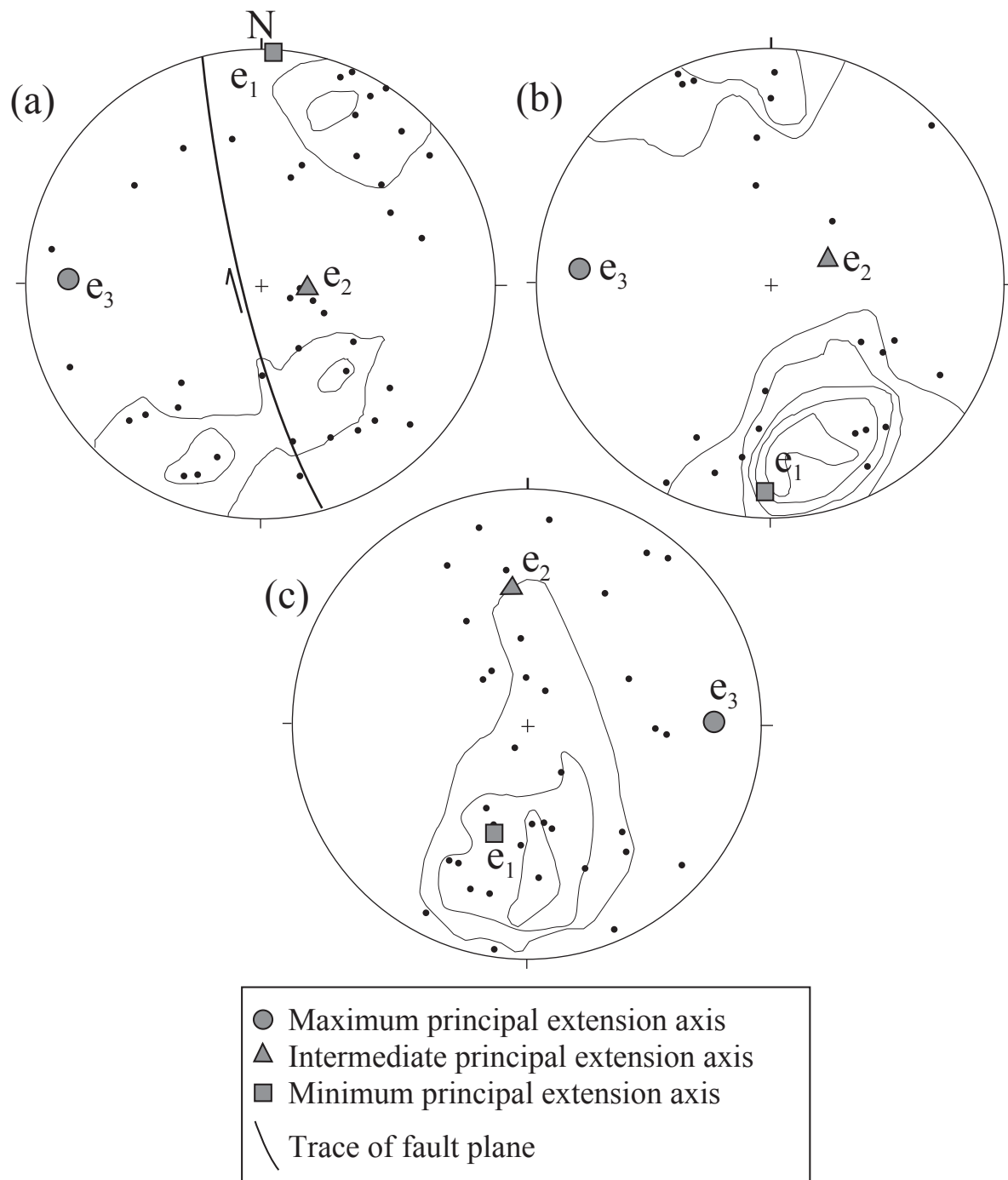


Figure 6
 Gray et al., 2004

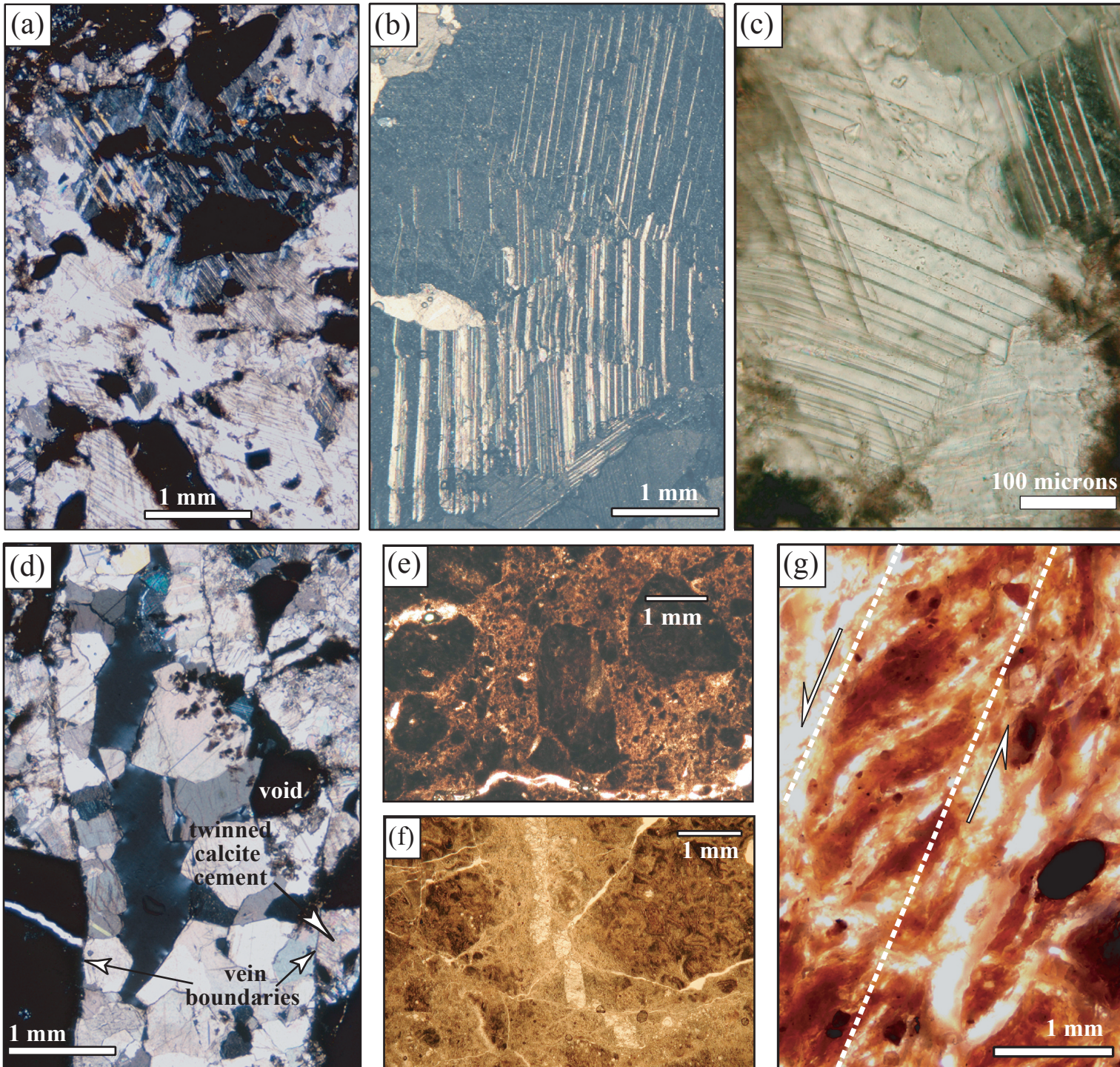


Figure 7
 Gray et al., 2004

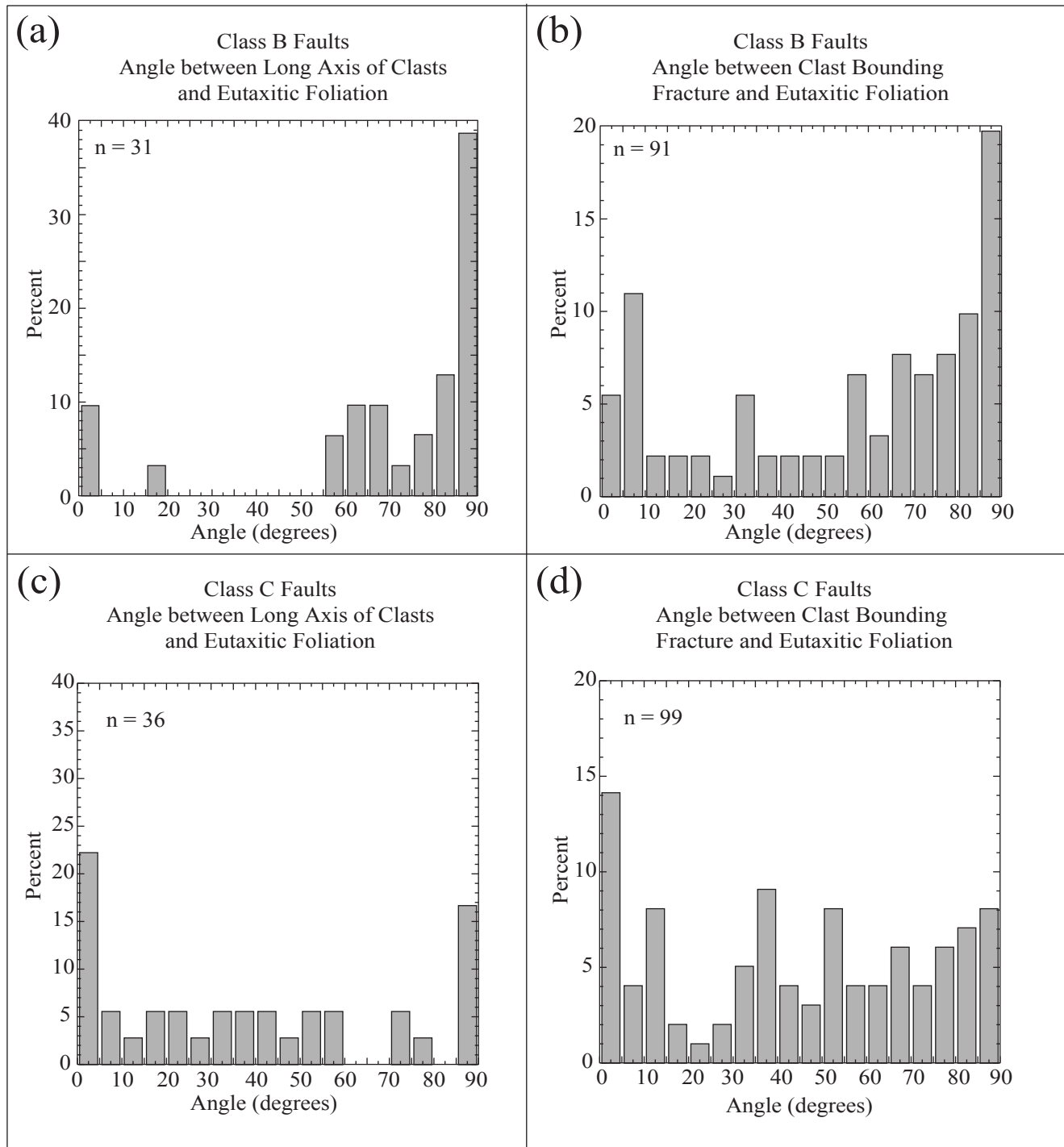


Figure 8
Gray et al., 2004

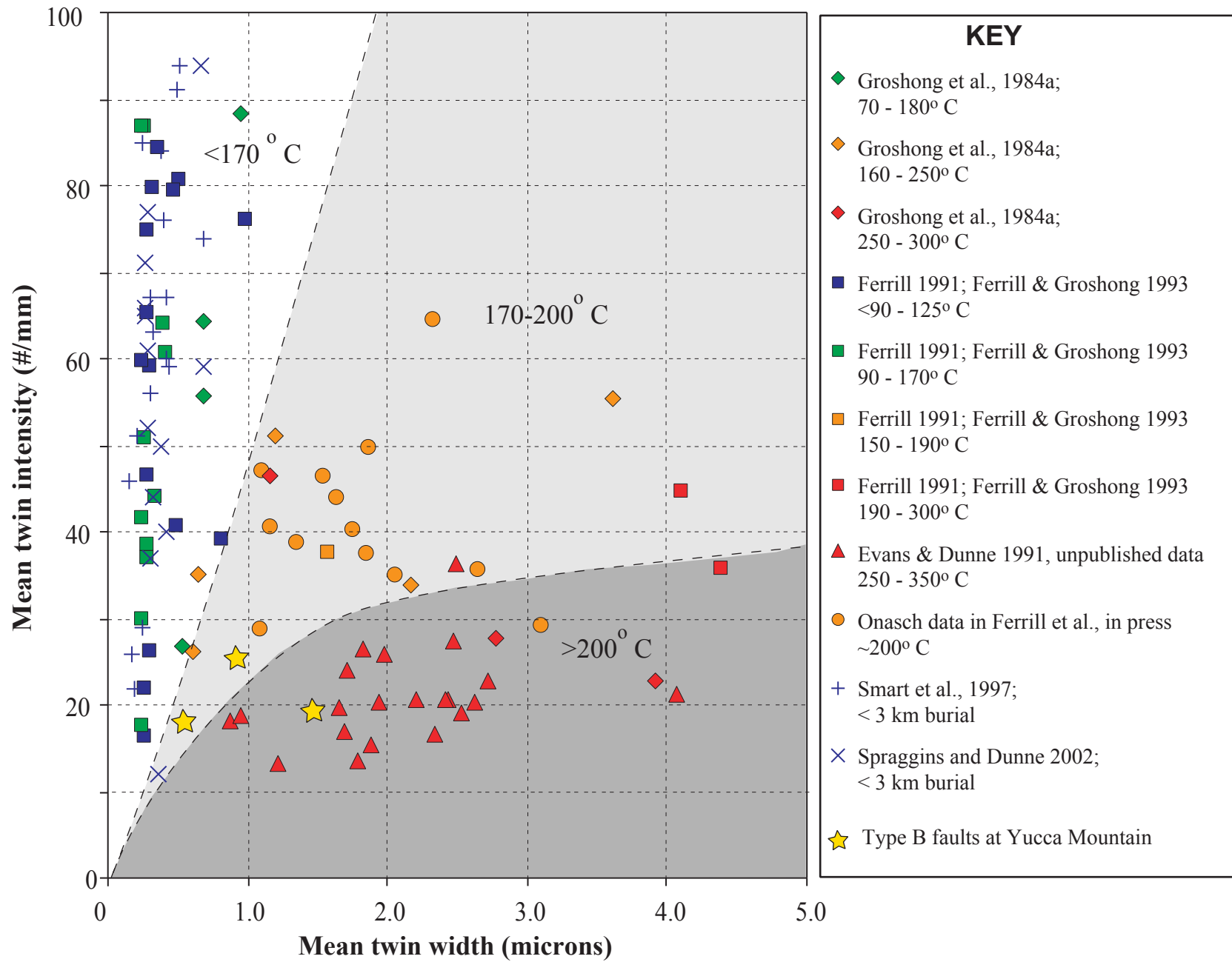


Figure 9
Gray et al., 2004

Increasing Fault Displacement

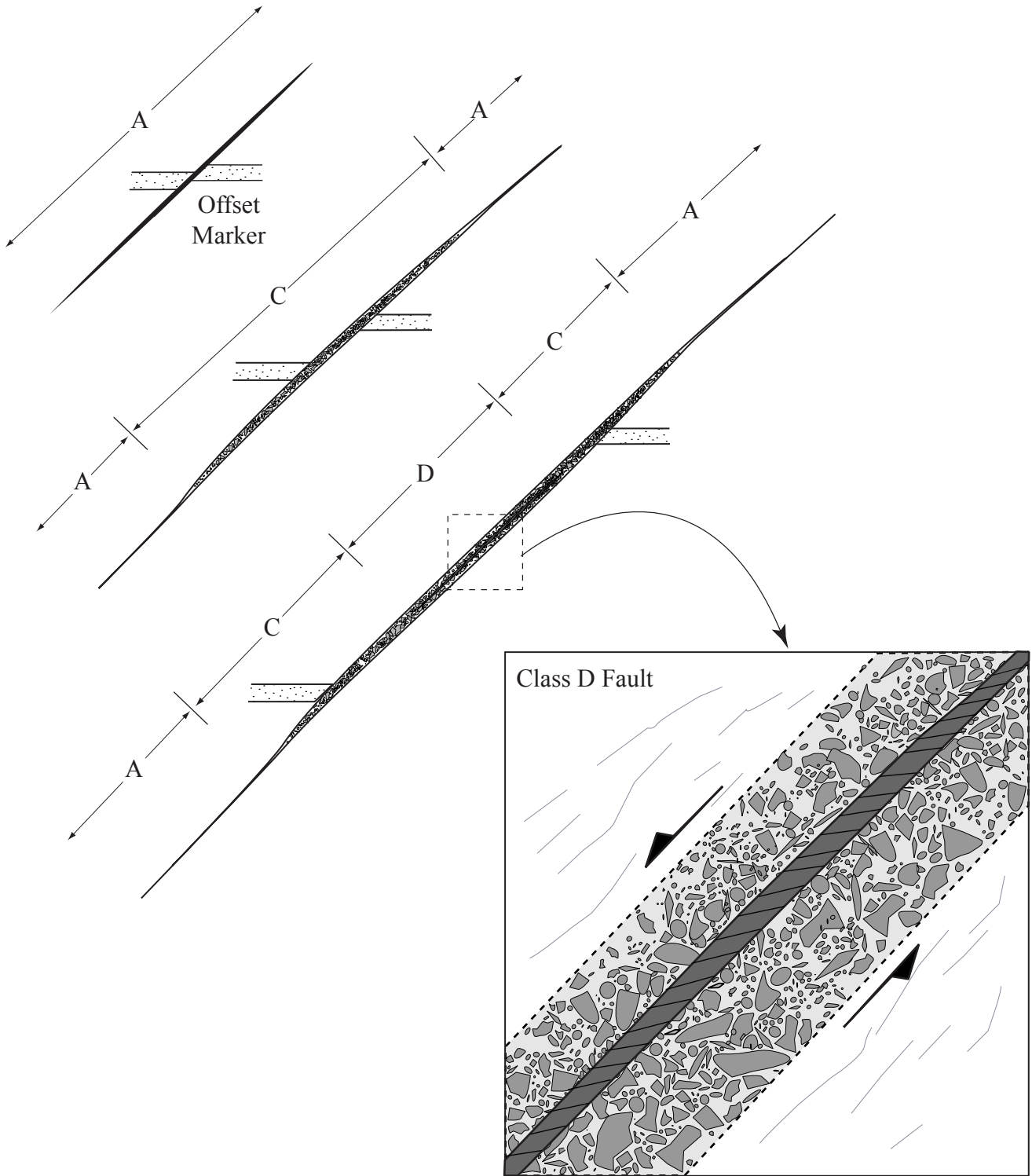


Figure 10
Gray et al., 2004

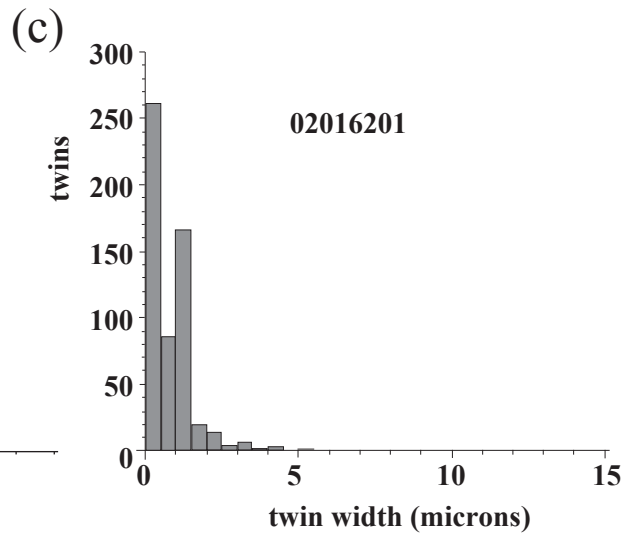
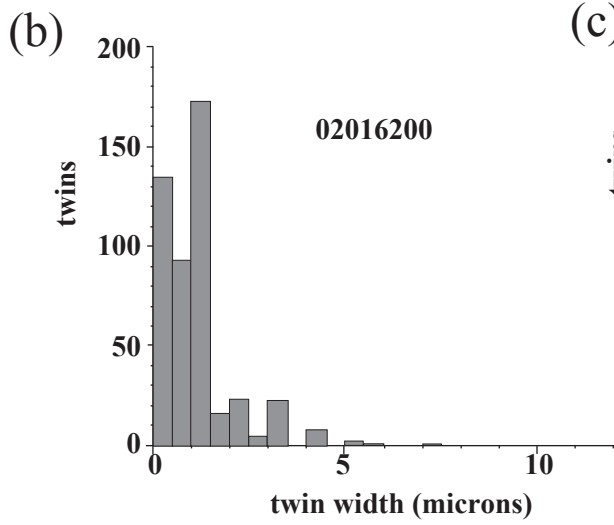
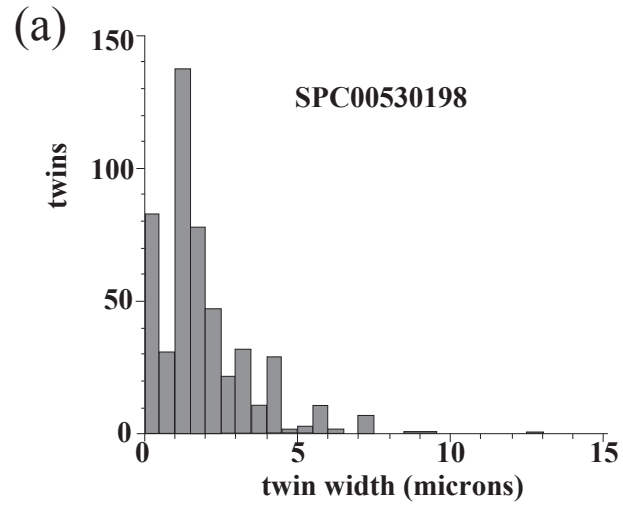


Table A1. Results of calcite e-twin analysis

Sample	02016200	02016201	SPC00530198	
N/n	28/23	45/36	49/40	
Thick N	324	235	406	
Thin N	135	262	82	
Width (μm)	0.90	0.51	1.41	
Intensity (mm)	25.62	18.26	19.75	
$\sqrt{J_2}$	1.747	0.286	2.090	
Principal Strains (% elongation)	e_1	1.491	0.300	1.665
	e_2	0.431	-0.031	0.680
	e_3	-1.923	-0.269	-2.345
error	0.302	0.191	0.437	
%NEV	4.34	25	17.5	

N is the number of measured twin sets and n is the number of twin sets analyzed after removing those with large deviations from expected values. Thick N and Thin N are the total number of measured thick and thin twins, within the twin sets. Width is mean twin width. Density is number of twins per mm. ($\sqrt{J_2}$) is the square root of the second invariant of the strain tensor. %NEV is the percent negative expected values with strains expressed as %.